JOURNAL OF PETROLOGY

Journal of Petrology, 2021, Vol. 62, No. 12, 1–30
doi: 10.1093/petrology/egab052
Advance Access Publication Date: 15 June 2021
Original Manuscript

OXFORD

Detrital Chromite from Jack Hills, Western Australia: Signatures of Metamorphism and Constraints on Provenance

Leanne G.Staddon[1]*, Ian J. Parkinson[1], Aaron J. Cavosie[2], Tim Elliott[1], John W. Valley[3], John Fournelle[3], Anthony I. S. Kemp[4] Steven B. Shirey[5]

[1]School of Earth Sciences, Wills Memorial Building, Queens Road, University of Bristol, Bristol BS8 1RJ, UK; [2]Space Science and Technology Centre and the Institute for Geoscience Research, School of Earth and Planetary Sciences, Curtin University, Perth, WA 6845, Australia; [3]Department of Geoscience, University of Wisconsin-Madison, Madison, WI 53706, USA; [4]School of Earth Sciences, University of Western Australia, 35 Stirling Highway, Perth, WA 6009, Australia; [5]Earth and Planets Laboratory, Carnegie Institution for Science, Washington, DC 20015, USA

*Corresponding author: Present address: School of the Environment, Geography and Geoscience, Burnaby Building, University of Portsmouth, Burnaby Road, Portsmouth PO1 3QL, UK. E-mail: Leanne.staddon@port.ac.uk

Received 27 April 2020; Accepted 6 June 2021

ABSTRACT

Detrital chromites are commonly reported within Archean metasedimentary rocks, but have thus far garnered little attention for use in provenance studies. Systematic variations of Cr–Fe spinel mineral chemistry with changing tectonic setting have resulted in the extensive use of chromite as a petrogenetic indicator, and so detrital chromites represent good candidates to investigate the petrogenesis of eroded Archean mafic and ultramafic crust. Here, we report the compositions of detrital chromites within fuchsitic (Cr-muscovite rich) metasedimentary rocks from the Jack Hills, situated within the Narryer Terrane, Yilgarn Craton, Western Australia, which are geologically renowned for hosting Hadean (>4000 Ma) zircons. We highlight signatures of metamorphism, including highly elevated ZnO and MnO, coupled with lowered Mg# in comparison with magmatic chromites, development of pitted domains, and replacement of primary inclusions by phases that are part of the metamorphic assemblages within host metasedimentary rocks. Oxygen isotope compositions of detrital chromites record variable exchange with host metasedimentary rocks. The variability of metamorphic signatures between chromites sampled only meters apart further indicates that modification occurred *in situ* by interaction of detrital chromites with metamorphic fluids and secondary mineral assemblages. Alteration probably occurred during upper greenschist to lower amphibolite facies metamorphism and deformation of host metasedimentary rocks at ~2650 Ma. Regardless of metamorphic signatures, sampling location or grain shape, chromite cores yield a consistent range in Cr#. Although other key petrogenetic indices, such as Fe_2O_3 and TiO_2 contents, are complicated in Jack Hills chromites by mineral non-stoichiometry and secondary mobility within metasedimentary rocks, we demonstrate that the Cr# of chromite yields significant insights into their provenance. Importantly, moderate Cr# (typically 55–70) precludes a komatiitic origin for the bulk of chromites, reflecting a dearth of komatiites and intrusive equivalents within the erosional catchment of the Jack Hills metasedimentary units. We suggest that the Cr# of Jack Hills chromite fits well with chromites derived from layered intrusions, and that a single layered intrusion may account for the observed chemical compositions of Jack Hills detrital chromites. Where detailed characterization of key metamorphic signatures is undertaken, detrital chromites preserved within Archean metasedimentary rocks may therefore yield valuable information on the petrogenesis and geodynamic setting of poorly preserved mafic and ultramafic crust.

Key words: Archean; chromite; Jack Hills; Narryer Terrane; provenance

INTRODUCTION

The detrital record of crustal evolution within the early Earth is dominated by analysis of the mineral zircon. This is particularly evident in the Narryer Terrane, within the Yilgarn Craton of Western Australia (Fig. 1). Here, Proterozoic to late Archean (Cavosie *et al.*, 2004; Crowley *et al.*, 2005; Rasmussen *et al.*, 2010; Wang & Wilde, 2018) metasedimentary rocks in the Jack Hills (Fig. 2) yield the oldest known fragments of terrestrial crust, individual grains of detrital zircon that yield ^{207}Pb–^{206}Pb ages up to 4374 ± 6 Ma (Compston & Pidgeon, 1986; Wilde *et al.*, 2001; Valley *et al.*, 2014). Despite isolated occurrences of Hadean detrital zircon elsewhere (e.g. Byerly *et al.*, 2018, and references therein), including Mt Narryer to the SW (Fig. 1; Froude *et al.*, 1983; Pidgeon & Nemchin, 2006), and rare examples of Hadean xenocrystic zircon (Nelson *et al.*, 2000; Wyche *et al.*, 2004; Iizuka *et al.*, 2006; Chaudhuri *et al.*, 2018), Jack Hills detrital zircons represent critically important remnants of Hadean (>4000 Ma) crust.

These zircons therefore provide a unique window into the Hadean Earth, and have subsequently been rigorously interrogated using numerous geochemical and isotopic techniques (e.g. Cavosie *et al.*, 2018). Previous investigations of Jack Hills zircons have broached a wide range of subjects, including Earth's ancient dynamo (Borlina *et al.*, 2020; Tarduno *et al.*, 2020), the origins of life (Bell *et al.*, 2015*a*) and the role of impacts within the early Earth (Bell & Harrison, 2013; Cox *et al.*, 2017). Despite intense study, what Jack Hills zircons tell us about the composition, evolution and subsequent destruction of their original host rocks is controversial, with conflicting hypotheses inferring vastly disparate geodynamic conditions within the early

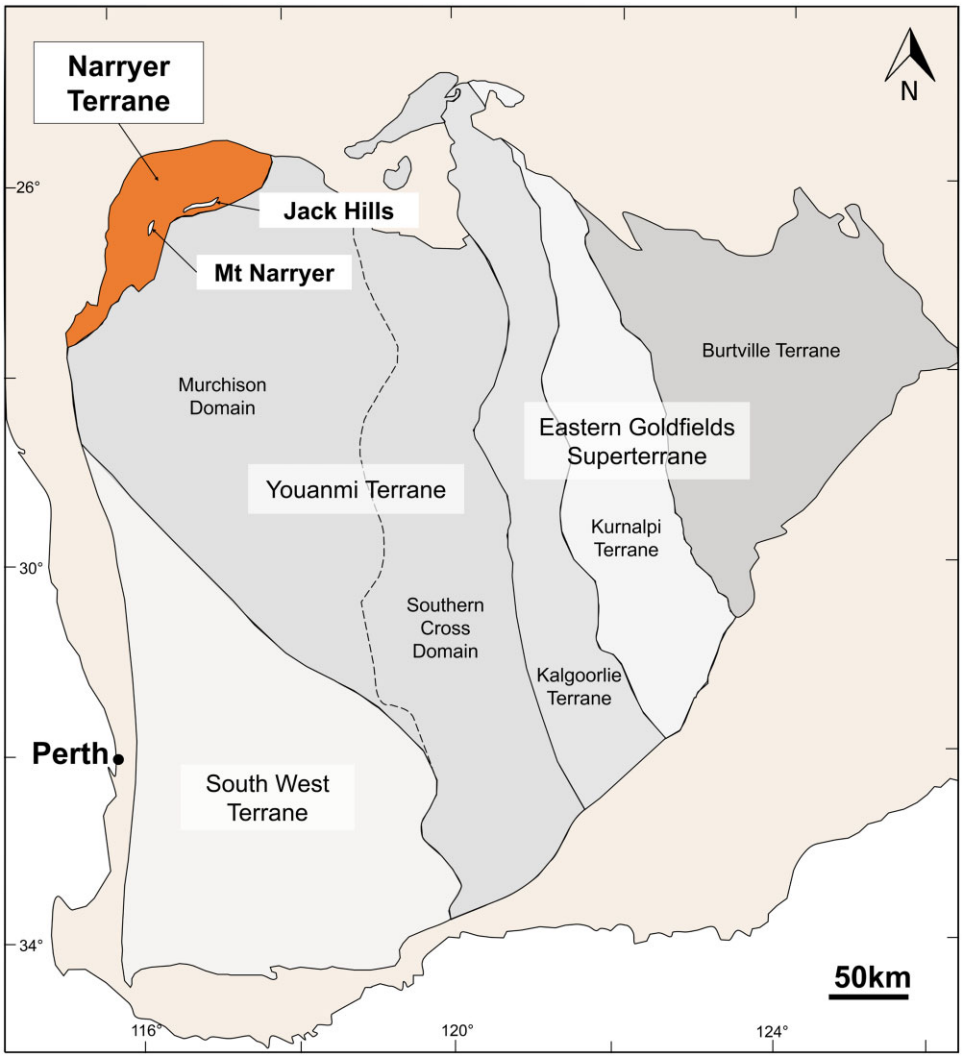

Fig. 1. Map of the Yilgarn Craton, Western Australia, showing the position of the Narryer Terrane, Jack Hills and Mount Narryer. Modified from Kemp *et al.* (2018) with terrane boundaries after Cassidy *et al.* (2006).

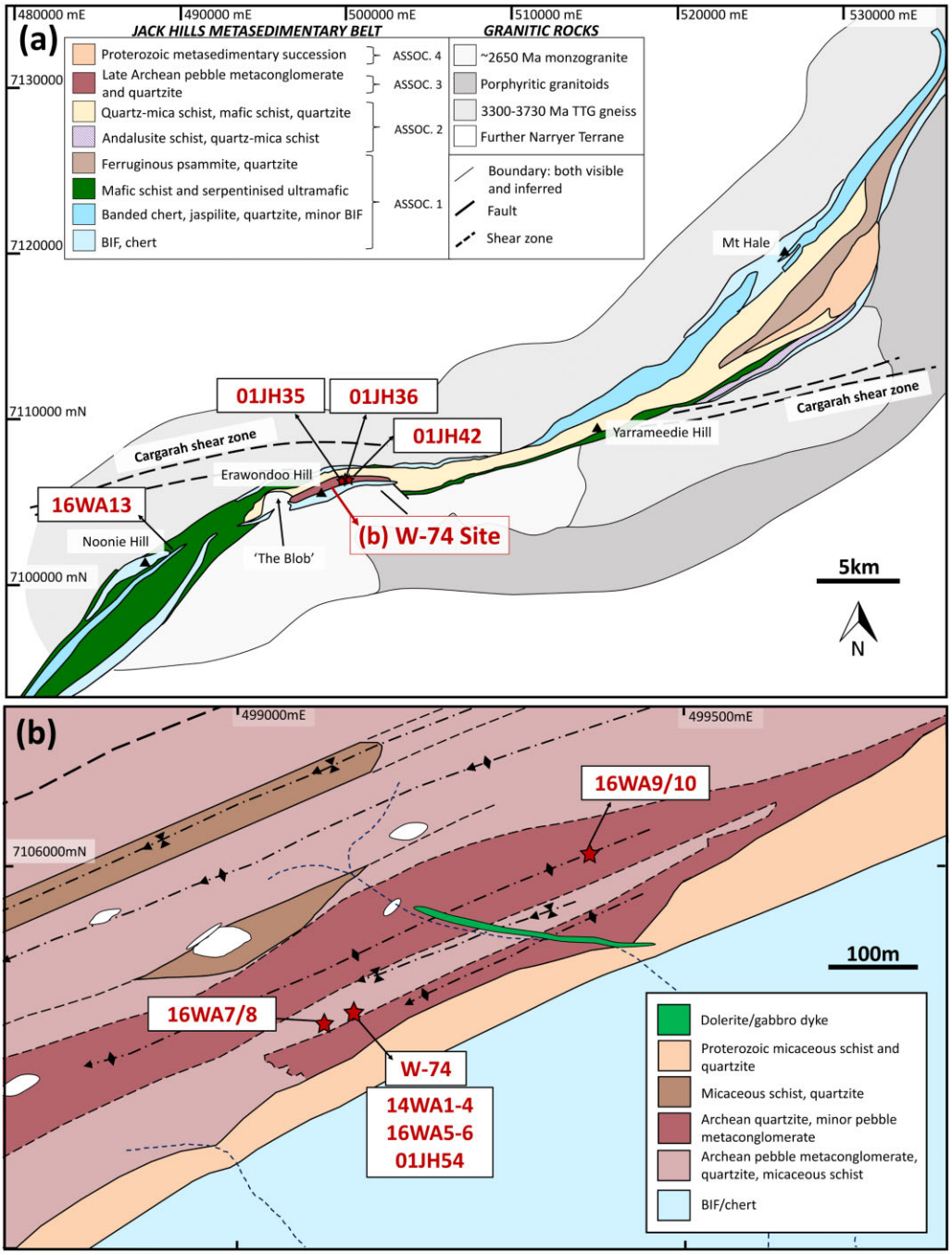

Fig. 2. (a) Simplified geological map of Jack Hills and surrounding quartzofeldspathic gneiss and granitoids with sampling locations, after Pidgeon & Wilde (1998) and Spaggiari *et al.* (2007). (b) Higher resolution geological map of sampling locations at and around the W-74 discovery site. Modified after Spaggiari *et al.* (2007). (See Methods and Materials for relative positions of samples from the W-74 site.)

Earth. Such hypotheses include a 'cool early Earth' (e.g. Valley *et al.*, 2002), the putative operation of plate tectonics (Harrison *et al.*, 2008, 2017; Bell *et al.*, 2014), production of zircon-bearing crust by internal reworking of mafic protocrust (Amelin *et al.*, 1999; Kemp *et al.*, 2010), or compositionally diverse protoliths (Wang & Wilde, 2018).

Although the Jack Hills zircon record yields valuable, if controversial, constraints on the evolution of felsic Hadean and Archean crust, detrital zircons provide little information on the evolution of contemporaneous mafic and ultramafic crust. This record is of particular importance, as emerging evidence indicates that mafic to ultramafic crust was the dominant compositional component of the Archean (e.g. Dhuime *et al.*, 2015; Kamber, 2015; Tang *et al.*, 2016). Evolved, zircon-bearing crust is therefore over represented within detrital records, in part owing to the poorer preservation

potential of mafic to ultramafic counterparts. Whereas the wider Yilgarn Craton is renowned for the presence of economically significant komatiites (Arndt *et al.*, 2008), the generation and evolution of mafic and ultramafic crust within the Narryer Terrane is poorly constrained by comparison. Indeed, the only well described >3100 Ma mafic and ultramafic crust within the entire Yilgarn Craton is the Eoarchean Manfred Complex (Wyche, 2007), a 3730 Ma disseminated layered intrusion within the Narryer Terrane (Fletcher *et al.*, 1988; Kinny *et al.*, 1988; Myers, 1988b; Rowe & Kemp, 2020).

However, the largely unexplored eroded remnants of mafic and ultramafic crust are ubiquitous within Jack Hills metasedimentary rocks, in the form of detrital chromites. Unlike zircon and other detrital phases observed at Jack Hills, chromite has a magmatic provenance restricted solely to mafic and ultramafic crust (Barnes & Roeder, 2001). Furthermore, chromites within their mafic or ultramafic protoliths are frequently used as a petrogenetic indicator, owing to systematic chemical variations in chromite formed under different tectonic conditions (Irvine, 1965, 1967; Dick & Bullen, 1984; Roeder, 1994; Barnes & Roeder, 2001; Kamenetsky *et al.*, 2001). Critically, the sequestration of platinum group elements (PGE) into spinel means that chromite is amenable to geochronology using Re–Os and Pt–Os decay systems (Shirey & Walker, 1998), potentially allowing a temporal framework of the generation of chromite-bearing mafic and ultramafic crust to be constrained from the detrital record. The value of detrital chromites for elucidating the provenance of magmatic protoliths has previously been demonstrated (e.g. Barnes & Roeder, 2001; Lenaz & Princivalle, 2005; Barkov *et al.*, 2013; Haugaard *et al.*, 2021; Lowe *et al.*, 2021), although additional care is required to quantify the effects of metamorphism on detrital chromite found within ancient terranes (Barnes, 2000; Colás *et al.*, 2014). Understanding how and when Jack Hills detrital chromites formed will therefore provide valuable information on the composition and petrogenesis of poorly described mafic and ultramafic crust that was potentially exposed at the time the Jack Hills sedimentary succession was deposited.

Here, we report major and minor element geochemistry of detrital chromites from 14 samples of metasedimentary rocks collected from within the Jack Hills (Fig. 2). This study combines data collected by two groups (University of Bristol, 14WA and 16WA samples; University of Wisconsin-Madison, 01JH samples), signifying a new direction compared with traditional provenance studies undertaken by analysis of detrital zircon. We highlight the effects of metamorphism on chromite mineral chemistry, discuss the retention of primary elemental and/or isotopic signatures, and propose a plausible provenance for detrital chromites. These grains enhance our understanding of the metamorphic history of the Jack Hills metasedimentary rocks and the distribution of mafic and ultramafic crust within the Archean upper crust at the time of deposition, and highlight the wider potential of detrital chromites for provenance studies of ancient mafic and ultramafic crust.

GEOLOGICAL SETTING

The Narryer Terrane

The Narryer Terrane is the most northwesterly terrane within the Yilgarn Craton of Western Australia (Myers, 1988a; Kemp *et al.*, 2018; Fig. 1), and has been interpreted as a deep crustal allochthon thrust onto the Youanmi Terrane (Nutman *et al.*, 1993), prior to or coincident with cratonic amalgamation (Kemp *et al.*, 2018). The terrane is dominantly composed of granitic lithologies, now largely preserved as quartzofeldspathic orthogneisses with >3 Ga protolith ages, with minor ultramafic and mafic intrusive rocks, and metasedimentary rocks (Myers & Williams, 1985; Williams & Myers, 1987; Myers, 1988a). Neoarchean (~2700–2650 Ma) granitic rocks are also abundant (Kemp *et al.*, 2018). Much of the Narryer Terrane has undergone high-grade, polyphase deformation, with amphibolite to granulite facies events at ~2700–2650 Ma forming the observed gneissic fabrics (Myers, 1988a; Kinny, 1990; Nutman *et al.*, 1991). There is evidence for previous high-grade thermal events, particularly at *ca.* 3300 Ma (Nutman *et al.*, 1991; Kinny & Nutman, 1996), and it has been postulated that the orthogneisses experienced multiple episodes of deformation and anatexis prior to late Archean metamorphism (Kinny & Nutman, 1996).

Despite complicated zircon geochronology (Pidgeon & Wilde, 1998), three dominant quartzofeldspathic orthogneiss units are identified within the Narryer Terrane (Kemp *et al.*, 2018). The Meeberrie gneiss is a biotite-rich migmatite that consists of 3670–3600 Ma monzogranitic and 3730 Ma tonalitic protoliths (Nutman *et al.*, 1991; Kinny & Nutman, 1996; Pidgeon & Wilde, 1998). The Eurada gneiss is a series of ~3480 Ma tonalitic gneisses that form a fault-bound lozenge west of Mount Narryer (Nutman *et al.*, 1991). The Dugel gneiss yields a well-constrained age of 3375 ± 26 Ma (Nutman *et al.*, 1991) and it is thought that its syenogranitic protoliths intruded the Meeberrie Gneiss as a series of sheet-like and pegmatitic bodies (Myers, 1988a; Kemp *et al.*, 2018).

The Meeberrie and Dugel gneiss host dispersed fragments of the Manfred Complex, a magmatically and tectonically dismembered and variably metamorphosed layered intrusion. The complex is dominantly amphibolitized gabbro and leucogabbro, with pyroxenite, metaperidotite and anorthosite (Williams & Myers, 1987; Fletcher *et al.*, 1988; Myers, 1988b; Rowe & Kemp, 2020). Relict igneous textures and layering are locally preserved (Kemp *et al.*, 2018). Zircon within Manfred Complex anorthosite and leucogabbro yields $^{207}Pb/^{206}Pb$ ages of 3730 ± 6 Ma (Kinny *et al.*, 1988; Kemp *et al.*, 2018), with other lithologies yielding Sm–Nd and Pb–Pb whole-rock (WR) ages of 3680 ± 70 Ma and 3689 ± 146 Ma, respectively (Fletcher *et al.*, 1988).

Spinel (spinel *sensu stricto* to picotite) and olivine chemical compositions are consistent with formation of the Manfred Complex within a thickened oceanic plateau; reduced, high Al–Ca–Fe picritic to tholeiitic basaltic parental melt compositions are thought to be derived from shallow partial melting of spinel lherzolite (Rowe & Kemp, 2020).

Jack Hills

The Jack Hills are located at the southern margin of the Narryer Terrane (Figs 1 and 2) and are a thin, ~70 km long belt, with a distinctly curvilinear shape produced by dextral shearing (Spaggiari, 2007). The Jack Hills belt is tectonically juxtaposed with the surrounding gneisses, except for localized intrusion of 2654 Ma monzogranite (also known as 'The Blob'; Pidgeon & Wilde, 1998; Spaggiari *et al.*, 2007; Fig. 2a), and has been interchangeably referred to as a greenstone belt (e.g. Spaggiari, 2007 ; Spaggiari *et al.*, 2007) or metasedimentary–supracrustal belt (e.g. Wang & Wilde, 2018). The Jack Hills largely consists of siliciclastic units, including metaconglomerate, quartzite and quartz–mica schist, with minor intercalated mafic and ultramafic rocks, banded iron formation (BIF) and chert. The presence of grunerite within BIF and hornblende within mafic schist indicates that at least portions of the belt have reached amphibolite facies metamorphism, whereas later greenschist facies metamorphism defines the dominant metamorphic signature of the belt (Spaggiari, 2007).

Deformation has tectonically disturbed and juxtaposed lithological associations, making an original stratigraphy difficult to discern. Spaggiari (2007) divided the belt into four associations determined by lithological variability (Fig. 2). Briefly, association 1 consists of interbedded BIF, chert and quartzite, mafic and ultramafic rocks, and black and white banded quartzites. Association 2 yields pelitic to semi-pelitic associations, now present as quartz–mica and andalusite schists, with accompanying mafic schist and quartzite. The presence of an S_1 cleavage and recumbent folding absent from other lithological units suggests that associations 1 and 2 were deformed prior to the deposition of association 3 and 4 (Spaggiari, 2007). Association 3 is restricted to the central region of the belt at Erawondoo Hill (Fig. 2), and was derived from mature, siliciclastic sediments interpreted to have been deposited within a deltaic alluvial fan (Spaggiari, 2007; Spaggiari *et al.*, 2007) between ~3050 and 2650 Ma (Crowley *et al.*, 2005; Rasmussen *et al.*, 2010). The discovery of Proterozoic detrital zircons (Cavosie *et al.*, 2004; Dunn *et al.*, 2005; Grange *et al.*, 2010) within the Jack Hills belt led to the recognition of association 4, which includes metasedimentary rocks deposited during the Proterozoic. Wang & Wilde (2018) observed interbedded siliciclastic units at the same apparent metamorphic grade but with both Archean and Proterozoic depositional ages, highlighting that the depositional and/or tectonic relationships of units 3 and 4 may be more complex than previously postulated.

Metasedimentary rocks within Jack Hills show clear indications of deformation; intense shearing is particularly evident within the anastomosing micaceous matrix, where a strong foliation is coincident with flattening and recrystallization of quartzite cobbles (Spaggiari, 2007). Thermal or fluid events within the Jack Hills belt occurred at ~3080, 2650, ~1850–1800 and 800 Ma (Spaggiari, *et al.*, 2007; Rasmussen *et al.*, 2010, 2011). Monazite–xenotime thermometry of secondary inclusions within detrital zircon yields temperatures of 420–475 °C (Rasmussen *et al.*, 2011), argued to represent peak upper greenschist to lower amphibolite facies metamorphism within association 3 metasedimentary rocks at ~2650 Ma (Rasmussen *et al.*, 2010). However, like the depositional ages of metasedimentary associations, the exact *P*–*T* conditions and timing of metamorphism within association 3 and 4 metasedimentary rocks are ambiguous (Kemp *et al.*, 2018). A Proterozoic event at ~1800 Ma (Spaggiari *et al.*, 2007; Rasmussen *et al.*, 2010) and a discrete event at 800 Ma (Rasmussen *et al.*, 2010, 2011) are of unknown metamorphic grade, but also coincide with formation of monazite and xenotime (Rasmussen *et al.*, 2010, 2011).

Metasedimentary rocks from Erawondoo Hill, chiefly oligomict pebble to cobble metaconglomerate and quartzite, are renowned for hosting Hadean detrital zircon (Compston & Pidgeon, 1986; Wilde *et al.*, 2001), with most studies focused on metasedimentary rocks at the W-74 'discovery site' (Fig. 2). Unsurprisingly, Jack Hills detrital zircons have been the subject of numerous publications and reviews (e.g. Harrison *et al.*, 2017; Cavosie *et al.*, 2018). Although a detailed description of the zircons is beyond the remit of this paper, it is important to note there is some debate surrounding the source rocks indicated by detrital zircon ^{207}Pb–^{206}Pb age distribution peaks, and thus the source of detritus. Although ^{207}Pb–^{206}Pb age peaks correspond to major units of the Narryer Terrane and the granitic lithologies surrounding Jack Hills (Nutman *et al.*, 1991; Pidgeon & Wilde, 1998), sources of more intermediate composition have also been suggested (Crowley *et al.*, 2005; Turner *et al.*, 2020). Additionally, the protoliths of >3800 Ma zircons are unknown, and may derive from a source exogenous to the Narryer Terrane. By extension, sources of detrital chromites external to the Narryer Terrane cannot be discounted. If detrital phases are derived from the Narryer Terrane, a further consideration is that both detrital zircon and chromite are present within quartzite clasts of the metaconglomerates (e.g. Grange *et al.*, 2010; Dare *et al.*, 2016). This demonstrates that detrital phases have undergone multiple sedimentary cycling events. It is therefore plausible that the source of detrital chromite had already been completely or partially eroded at the time of deposition of the Jack Hills sediments (3050 to 2650 Ma), and therefore may not represent the distribution of mafic and ultramafic crust

during the late Archean (Crowley *et al.*, 2005; Rasmussen *et al.*, 2010).

Despite concerted interest in detrital zircon at Jack Hills, detrital chromites within the same metasedimentary rocks have garnered less attention. Detrital chromites with low Mg# [100 × molar Mg/(Mg + Fe^{2+})] and elevated ZnO and MnO were reported by Cavosie *et al.* (2002) for grains from the W-74 site; comparable major element compositions were described by Dare *et al.* (2016) in analyses of detrital chromites ~1 km to the NW of this locality. Dare *et al.* (2016) proposed that low MgO contents of chromites precluded derivation of Jack Hills detrital chromites from komatiites, and that both chromite and Fe–Ni-sulphides observed within quartzite clasts are the erosional products of at least one layered intrusion. Unpublished Re–Os model ages (T_{MAs}) of 3500 to 3200 Ma were reported by Valley *et al.* (2005) for the same population of chromites as described by Cavosie *et al.* (2002). These data suggest that the analysed detrital chromites are at least Palaeoarchean in age, and highlight the potential preservation of robust Re–Os systematics through peak metamorphism within the Jack Hills.

METHODS AND MATERIALS

Sample collection and preparation

Sampling locations of metasedimentary rocks are shown in Fig. 2. Seven samples of pebble metaconglomerates (14WA1-4, 16WA5-6 and 01JH54) were collected from within 10 m of the W-74 site (Wilde *et al.*, 2001) at Erawondoo Hill (Fig. 2b). A further sample of pebble metaconglomerate (16WA8) and a quartzite (16WA7) were collected along-strike *ca.* 35 m to the WSW. Two pebble metaconglomerates (16WA9-10) were sampled from a prominent ridge across the valley to the NE. Three samples were collected further to the NE of the W-74 site. 01JH35 is a metaconglomerate sampled ~800 m to the NE of the W-74 site. 01JH36, collected *ca.* 200 m to the ENE of 01JH35, is a quartzite with discrete, millimeter-scale heavy mineral bands (Cavosie *et al.*, 2004). Finally, 01JH42 is a pebble metaconglomerate sampled in the eastern transect of Cavosie *et al.* (2004). Petrographic sample descriptions of metasedimentary rocks and their detrital mineral assemblages are provided in Supplementary Data 1; supplementary data are available for downloading at http://www.petrology.oxfordjournals.org. Although fuchsite-rich (muscovite with >1 wt% Cr_2O_3; Challis *et al.*, 1995) metasedimentary rocks were largely collected to yield the highest concentrations of chromite grains, fuchsite is not abundant within 01JH36, 16WA6 and 16WA10.

Two chromite-bearing ultramafic rocks from within the Narryer Terrane are also included, with descriptions and sampling locations provided within Supplementary Data . Sample 13TKN22 is a metaperidotite from the 3730 Ma Manfred Complex, collected from NE of Mt Narryer and *ca.* 60 km SW of the Jack Hills. Sample 16WA13 is a heavily recrystallized ultramafic rock of unknown age sampled from the SW limb of Jack Hills (Fig. 2a); this sample is part of association 1 of Spaggiari (2007) and so is probably >3000 Ma.

Chips of Narryer Terrane ultramafic rocks were mounted in epoxy for petrographic study and identification of chromite. Chromites from samples 14WA, 16WA, 01JH35 and 01JH42 were separated using standard crushing and separation procedures, then sieved to yield size fractions of ≤500 μm for analysis. 01JH36 and 01JH54 chromites were separated by electric pulse disaggregation (EPD). 14WA1-4 heavy minerals were concentrated using the Wilfley table, where a hand-magnet was used to remove highly magnetic phases, followed by heavy liquid separation. 16WA5-10 separates were concentrated via panning and underwent no magnetic separation. 01JH chromites were concentrated using heavy liquids and a Frantz magnetic separator. Although magnetic separation of 14WA1-4 and 01JH samples may preferentially remove chromites with rims of ferritchromit [$Fe^{2+}(Fe^{3+},Cr)_2O_4$] or magnetite, the absence of such rims in 16WA (which did not undergo magnetic separation), within thin sections, and across hundreds of studied grains indicates that ferritchromit or magnetite do not represent a constituent phase within the Jack Hills chromite population. Chromites were picked by hand, separated by sample location, grain size and rounding shape, and mounted in epoxy. Detrital grains within a thin section of 14WA2 were also analysed, as were chromite grains liberated via HF leaching of quartzite cobbles from 14WA2 and 16WA5. No chemical differences between chromites present within quartzite cobbles or matrix were observed, so they are discussed together below.

Chromite mineral chemistry

14WA, 16WA and 13TKN22

Chromites were imaged using reflected light microscopy and/or back-scattered electron (BSE) imaging using a Hitachi S-3500N scanning electron microscope at the University of Bristol. Chromite major elements were determined from individual spots and line scans using the Cameca SX100 electron microprobe at the University of Bristol. Chromium, Al, Fe, Mg, Zn, Mn, Ti, V, and Ni abundances in chromite were determined using a 20 kV accelerating voltage, a 10 nA beam current, 1 μm beam diameter, and a PAP matrix correction. Silicon, Na and Ca were included within the set-up to monitor any silicate contamination; analyses with >0.15 wt% oxide of these elements were omitted. Counting times were 30 s for Cr, Fe, Al and Zn and 60 s for Ti, Ca, Mg, Na, Mn, V, Si and Ni, with the following standards used for instrument calibration: Cr_2O_3 (Cr), albite (Al and Na), ilmenite (Fe and Ti), St John's olivine (Mg and Si), Zn metal (Zn), Mn metal (Mn), V metal (V), Ni metal (Ni) and wollastonite (Ca). The overlap of Ti Kβ on V Kα was corrected either via analysis of V-free $SrTiO_3$ or using high-resolution slits. No resolvable

variability in the V_2O_3 contents of chromite or chromite secondary standards was observed between the two set-ups. Typical detection limits, expressed in ppm, were Cr (260), Al (250), Na (450), Fe (320), Ti (120), Mg (250), Si (180), Zn (400–500), Mn (300), V (200), Ni (350) and Ca (140).

Four spinel reference materials (8316, 8311, 79-1 and 8315), well characterized for $Fe^{3+}/\Sigma Fe$ using both electron probe microanalysis (EPMA) and Mössbauer analysis from Wood & Virgo (1989), were analysed in-run to monitor the integrity of EPMA measurements. Long-term reproducibility of major elements (Al, Cr, Fe, Mg) within reference materials 8316 and 8311, which possess the most comparable mineral chemistry to samples, is <1.2 wt% (2σ). The method of Droop (1987) was employed to calculate the ferric iron content of chromite by stoichiometry. The determined $Fe^{3+}/\Sigma Fe$ [molar $100 \times Fe^{3+}/(Fe^{3+} + Fe^{2+})$] of 8316 ($0.21 \pm 0.07$; 2σ) and 8311 ($0.17 \pm 0.06$; 2σ), measured across multiple analytical sessions, are in good agreement with reported values. After correction for ferric iron, 14WA4, 16WA6 and 16WA9-10 yielded chromite with systematically low totals, typically between 97 and 98 %, despite other analyses within the same run yielding good totals. The cause of low totals within these samples is unknown but may reflect non-stoichiometry, probably owing to site vacancies. Fe_2O_3 contents of chromite should therefore be considered minimum abundances. Chromites with totals of 97.5–102 % from 14WA4, 16WA6 and 16WA9-10 are included, whereas measurements from other samples are restricted to those that yield totals of 98–102 %.

01JH samples

EPMA was undertaken at the University of Wisconsin-Madison Department of Geoscience using a CAMECA SX51 electron microprobe equipped with Probe for EPMA software. Analyses were conducted at 20 kV, using a focused electron beam with a 20 nA beam current. Counting times for all elements were 10 s on peak and a total of 10 s on off-peak background positions. The matrix correction was the PAP procedure. PHA differential was used for Al and O, whereas other elements were measured in integral mode. Oxygen was determined with a 60 Å 2d PC0 diffractor crystal, whereas Si, Al and Mg were acquired on TAP, Ti and Cr on PET, and V, Mn, Fe, Ni, Cu and Zn on LIF. Overlap corrections were made on Al for Cr, Ni and Ti, on V for Ti, on Fe for Mn, and on O for Cr. The following standards were used for instrument calibration: USNM Chromite (Cr, Al, Mg, O), Harvard University hematite (Fe), synthetic tephroite (Mn, Si), V_2O_5 (V), rutile (Ti), Ni_2SiO_4 (Ni), $ZnAl_2O_4$ (Zn) and Cu_2O (Cu). Typical detection limits, expressed in ppm, were Cr (290), Al (260), Fe (540), Ti (120), Mg (260), Si (200), Zn (540), Mn (400), V (300), Ni (360) and Cu (450).

EPMA results were processed using two methods. In the first, oxygen measurements were omitted and analyses were processed using the same techniques as for 14WA and 16WA; namely, calculation of ferric iron by stoichiometry using the method of Droop (1987), and exclusion of analyses with >0.15 wt% SiO_2 and totals of <98 %. In the second method, cations and measured oxygen were converted into molar proportions, and the ferrous/ferric ratio of iron was adjusted to balance the negative charge from measured O. This technique assumes Fe is the only multivalent cation present (e.g. Cr is present as Cr^{3+}, V as V^{3+} and Mn as Mn^{2+}) and that site vacancies are negligible. The latter scenario is unlikely to be true within altered Cr-rich spinel (see Kamperman *et al.*, 1996), and so ferric iron compositions determined by the second method represent maximum values. For consistency, data calculated using stoichiometry are presented within the main text, whereas analyses processed using measured O are shown in Supplementary Data 2.

Oxygen isotope analyses

Chromite grains from samples 01JH36, 01JH42 and 01JH54 were analysed for oxygen isotope ratio by laser fluorination at the University of Wisconsin-Madison Department of Geoscience. A total of 35 analyses of oxygen isotope ratio in chromite were made using gas source mass spectrometry with BrF_5 and a 32 W CO_2 laser (Valley *et al.*, 1995). Chromite data were corrected for accuracy with the UWG-2 garnet oxygen standard, which was analysed multiple times at the beginning of the session (Valley *et al.*, 1995). The reproducibility of UWG-2 per session ranged from ±0.07 to ±0.11 (2σ; Supplementary Data 1 Table 2). Samples of chromite were first sieved into seven size fractions, ranging from 105–149 to >500 μm (Supplementary Data 1 Table 3). At least three size fractions were analysed from each sample, with two to three aliquots analysed from each size fraction. Aliquots of chromite were prepared by soaking detrital grains in concentrated HF at room temperature overnight. Each ~2 mg aliquot of chromite thus consisted of hundreds of clean detrital grains. Values are reported in standard per mil notation relative to V-SMOW (Vienna Standard Mean Ocean Water).

RESULTS

Chromite morphology and inclusion assemblages

Jack Hills detrital chromites are typically ≤500 μm grains of variable morphology (Fig. 3a) that are enclosed by, or closely associated with, fuchsite within quartzite or metaconglomerate matrix (Fig. 3b and c). Finer (≤100 μm) chromite grains have previously been reported within metaconglomerate quartzite cobbles (Dare *et al.*, 2016), but were uncommon in samples of this study (Fig. 3), although HF leaching of quartzite cobbles liberated a small number of grains ($n = 12$). Many

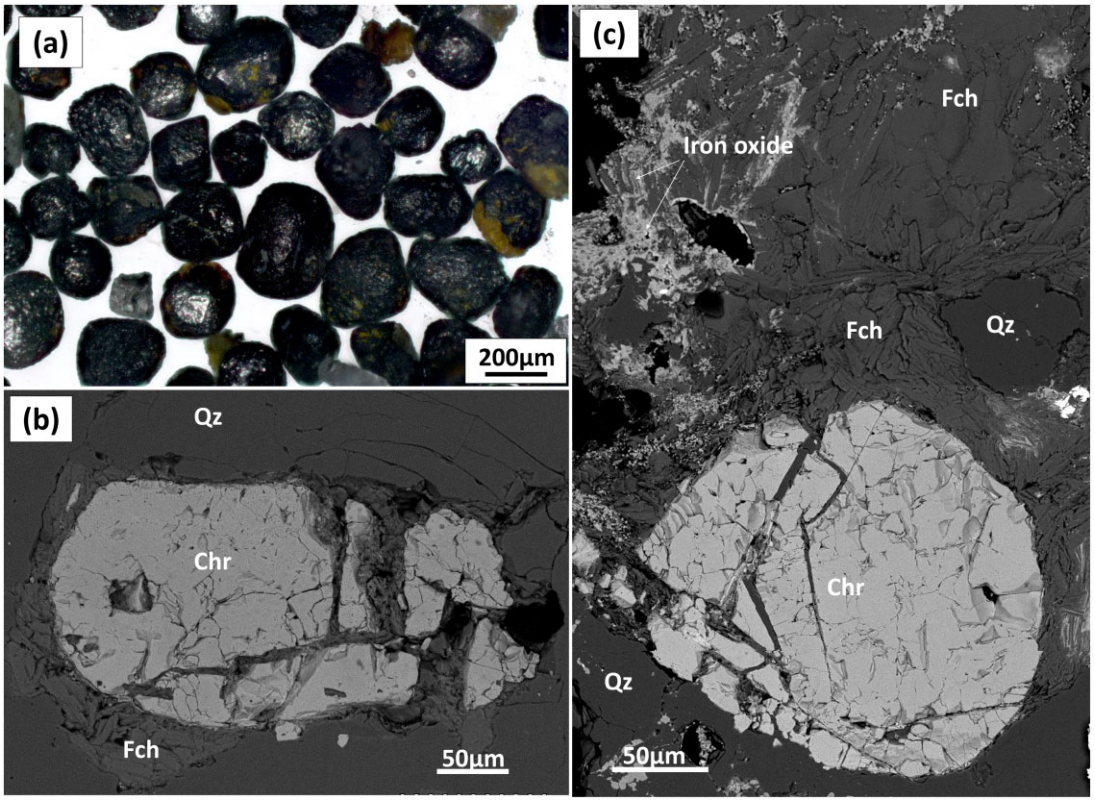

Fig. 3. Jack Hills detrital chromites. (a) Optical microscope image illustrating *ex situ* variably rounded morphologies of chromite grains. (Note the green–brown fuchsite.) (b) BSE image of chromite observed *in situ* within quartzite cobble. Despite isolation from metaconglomerate matrix the cobble has been infiltrated by secondary Cr-muscovite. (c) BSE image of complex and ragged boundaries between chromite and fuchsite within metaconglomerate matrix. Grain heavily fractured on its southern margin. Chr, chromite; Qz, quartz; Fch, fuchsite. Iron oxides are likely magnetite or goethite, but have not been analysed by EPMA.

chromites show textural evidence of sedimentary transport, including abrasion and rounding of broken surfaces. Chromite derived from Jack Hills metasedimentary rocks occurs as euhedral octahedra (EO), rounded octahedra (RO) or rounded grains (RC: rounded chromite) (Fig. 3a). EO yield minimal rounding on two or fewer faces, with many euhedral grains showing little or no evidence of sedimentary transport. RC grains demonstrate limited evidence of original habit on two or fewer faces, and are often present as highly spherical morphologies. RO are chromites with morphologies intermediate to EO and RC, and are the most abundant morphology. More quartzitic lithologies possess a greater proportion of euhedral grains. 16WA9 and 16WA10, sampled furthest from the W-74 site, yield a more bimodal distribution with chromite dominantly RC and minor EO.

A range of internal textures are present (Fig. 4), with grains often heavily cracked and displaying ragged or lobate boundaries with surrounding fuchsite (Fig. 3c). Fractures occasionally display distinct polygonal morphologies (Fig. 4b), and larger fractures may be filled with quartz, fuchsite, and Fe-oxide. Distinct 'pitted' textural domains within chromite reveal the presence of typically $\leq$10 µm inclusions of dominantly quartz and fuchsite (Figs 4 and 5). Rare porous textures with $\geq$30 µm inclusion assemblages may occasionally account for the majority of the grain (Fig. 4e and f). Both pitted and porous domains are conspicuous at chromite rims or adjacent to cracks, and particularly where chromite is enclosed by fuchsite. Fine laths of rutile, often showing apparent alignment to chromite crystallographic directions, are also commonly associated with pitted and porous domains (Figs 4f and 5a). Isolated monomineralic and polyphase silicate and oxide inclusions present within chromites are typically globular or anhedral in habit (Fig. 5), but may more rarely possess subhedral to euhedral morphologies (Fig. 5a and d). Inclusions associated with fractures and crack-filling assemblages of quartz, fuchsite and rutile (Fig. 5a, b and e) are often accompanied by other fine-grained (typically $\leq$10 µm) phases, including Fe-oxide (Fig. 5b), Fe-sulphide (Fig. 5c), and rarer monazite (Fig. 5f).

Chromite mineral chemistry

Representative analyses of detrital chromites from each metasedimentary sample location are presented in Table 1, and the full EPMA dataset is available in Supplementary Data 2. Chromite major element abundances show no variation with grain size or shape (Supplementary Data 1 Figs 9 and 10) but

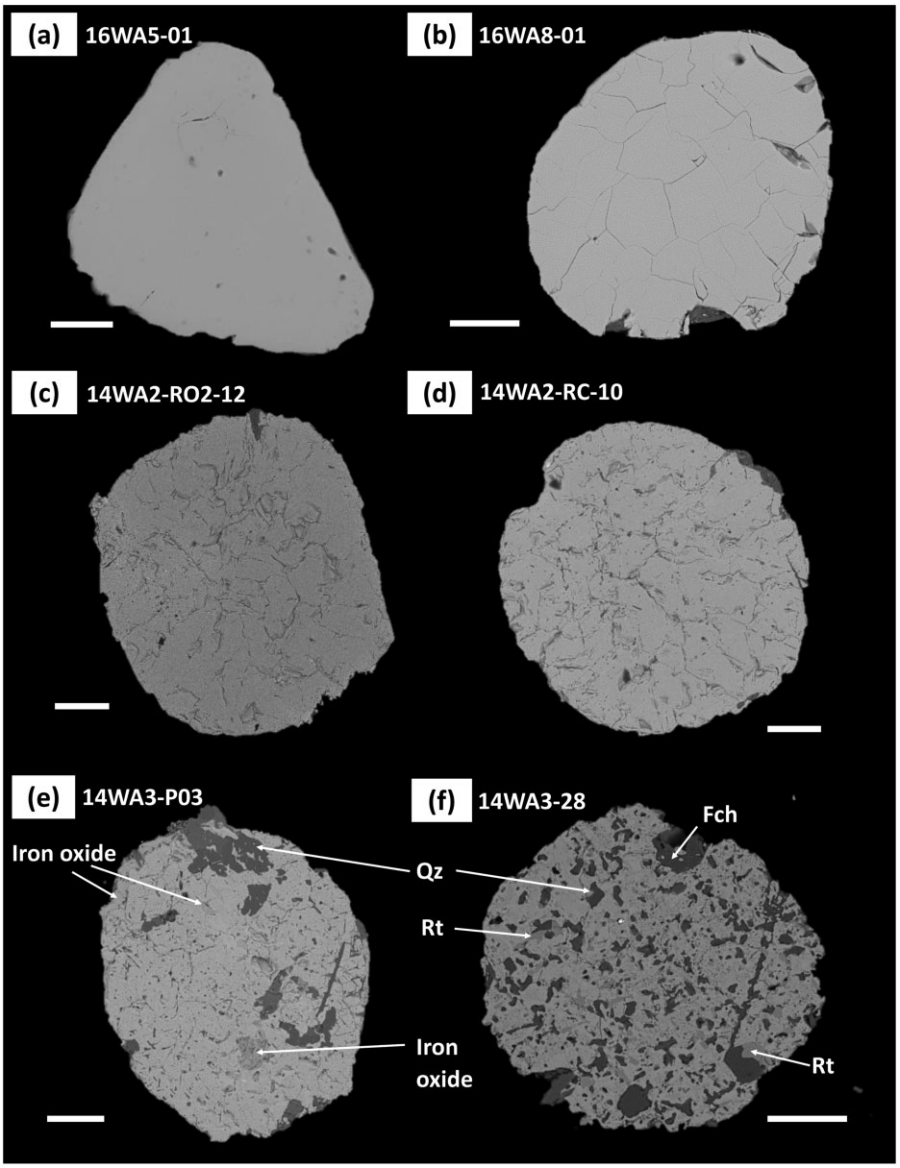

Fig. 4. BSE images showing chromite textural variation. All scale bars represent 50 μm. (a) Smooth with minimal fracturing. (b) Polygonal fracturing, no pitted domains. (c) Fractured with very fine pitted domains. (Note coarser pores, with pitted domains localized to edges and near fractures.) (d) Fractured with increasingly pitted textures, often away from obvious fractures. (e, f) Porous chromite, fractures apparently lost or infilled by secondary material. Secondary material often aligned. Qz, quartz; Fch, fuchsite; Rt, rutile. Iron oxides are probably magnetite, but have not been analysed by EPMA.

differ systematically between sampling locations (Figs 6 and 7).

Sample variability (Ti^{4+} and divalent cations; Fe^{2+}, Mg^{2+}, Zn^{2+}, Mn^{2+}, and Ni^{2+})

Chromites from all sampled metasedimentary rocks yield elevated ZnO (up to 13 wt%) and MnO (up to 4.4 wt%), coupled with low Mg# (typically ≤30; Fig. 6). Generally, samples with increasingly elevated ZnO yield lower and more homogeneous Mg# (Fig. 6a). 14WA2 chromites possess the lowest wt% ZnO (average ZnO 1.23 wt%) and largest range of Mg#, with a single grain (14WA2-PB-46) yielding Mg# of up to ~30. Unusually elevated MnO contents are present in 01JH35, where chromites yield >3.5 wt% MnO (Fig. 6b). No variation of MnO with Mg# is apparent (Fig. 6b), although some 16WA samples show variance between ZnO and MnO (Fig. 6d).

TiO_2 is typically <1 wt% (Fig. 6c). Individual analyses where TiO_2 is above 1 wt% correlate with areas where laths of rutile are present, and are omitted from consideration. Elevated TiO_2 of ≥1 wt% is most apparent within lower Cr# [100 × molar Cr/(Cr + Al)] grains (Fig. 7). As the bulk of analyses possess ≤0.3 wt% TiO_2, this suggests that analyses yielding TiO_2 >0.3 wt% may also overlap with rutile laths. However, many chromites with ~0.3–0.8 wt% TiO_2 show no evidence of rutile laths in BSE images. NiO within grains is largely below the quantification limit of ~0.04 wt%.

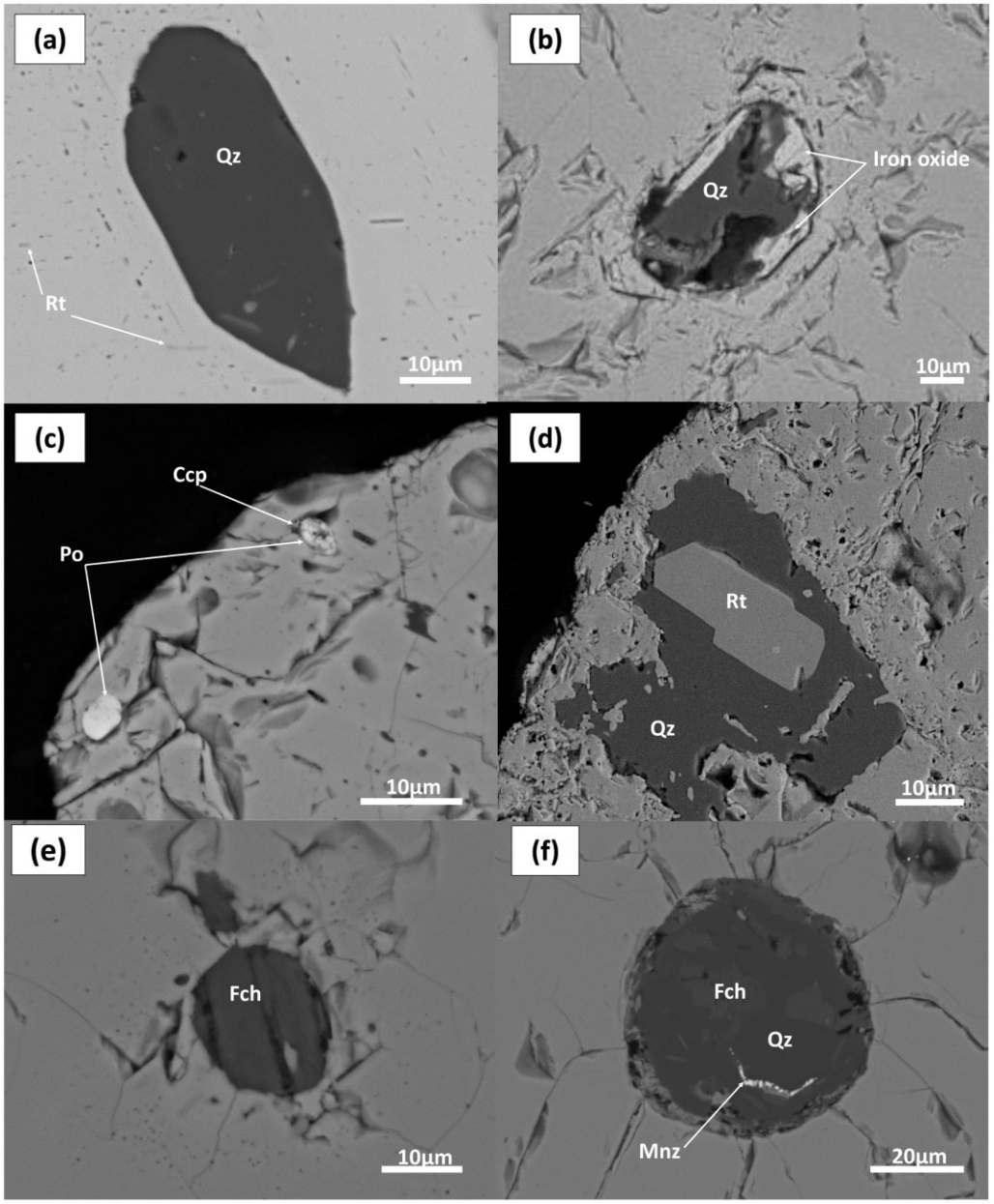

Fig. 5. BSE images of inclusion assemblages. (a) Isolated euhedral–subhedral quartz (Qz). Brighter crystallites in quartz are rutile, an Mg-silicate, and phosphate. The surrounding pitted domain including darker quartz and medium-grey rutile (Rt) laths, but an absence of fractures should be noted. (b) Isolated polyphase assemblage of quartz and iron oxide. (c) Subhedral Fe-sulphide within pitted domain of chromite; pyrrhotite (Po) and chalcopyrite (Ccp) (outlined). (d) Euhedral rutile within quartz (note the ragged boundaries of quartz and surrounding pitted domain). (e) Anhedral inclusion of fuchsite. (f) Globular inclusion of quartz and fuchsite with monazite (note the expansion cracks radiating from inclusion).

Sample variability (trivalent cations: Cr^{3+}, Al^{3+}, V^{3+}, Fe^{3+})

Despite considerable variability of divalent cation contents between sampling locations, detrital chromites show a similar range in Cr# between samples (Fig. 7). Chromites yield moderate to high and variable Cr# of 48–82, with the bulk of chromites displaying Cr# of 54–66 (Fig. 7a). The apparent smaller range of Cr# in chromites with higher wt% ZnO is probably a sampling bias owing to fewer analyses. V_2O_3 was not measured for 16WA5-7, but where measured is present at 0.05–0.37 wt% and shows no inter-sample variability. Jack Hills detrital chromites yield low calculated Fe_2O_3 contents; the bulk of the population contains $\leq$2 wt% Fe_2O_3, although analyses with up to 8 wt% Fe_2O_3 are present. This results in highly variable $Fe^{3+}/\Sigma Fe$ ratios of 0–20 (Fig. 7d). Many chromites yield non-stoichiometric compositions (e.g. deviation from $A^{2+}B_2^{3+}O_4$), shown by cation totals of less than three when normalized to four oxygens. This probably reflects cation vacancies (e.g. Kamperman *et al.*, 1996), and results in an underestimation of ferric iron contents by stoichiometric

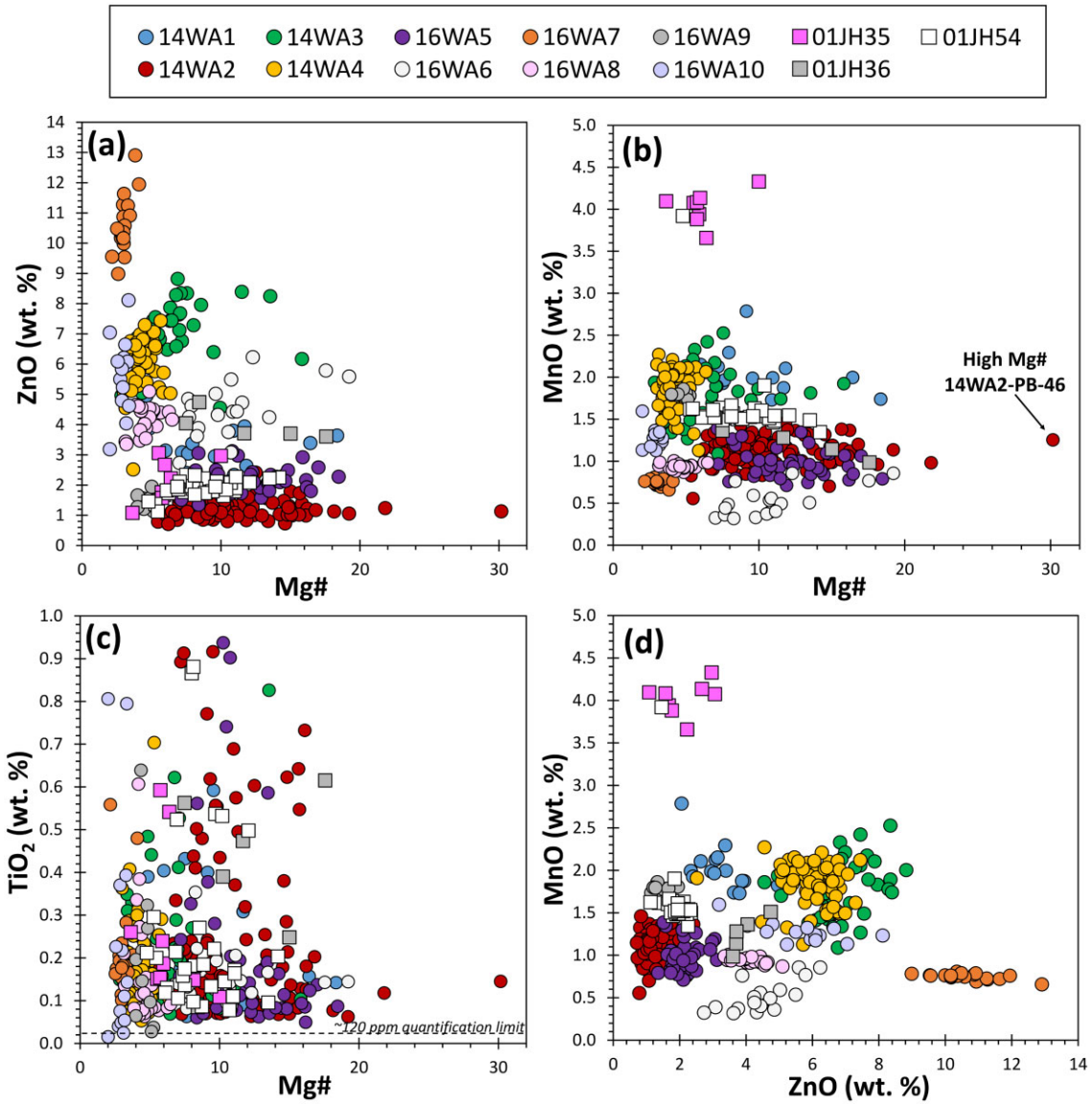

Fig. 6. Variation of Mg#, ZnO, MnO and TiO_2. Each data point is separated by sample and represents a core or near-core composition of chromite. (a) ZnO vs Mg#. (b) MnO vs Mg#. (c) TiO_2 vs Mg#. Most grains yield low TiO_2 of <0.25 wt%. It is likely that some analyses above this value overlapped with subsurface rutile laths. However, some grains with >0.25 wt% TiO_2 show no evidence of rutile laths. TiO_2 >1 wt% clearly represent overlap with rutile laths, so are omitted. (d) MnO vs ZnO. Anomalously high Mn within 01JH35.

calculations (Droop, 1987). Non-stoichiometry also affects analyses conducted by direct measurement of oxygen (Supplementary Data 2); analyses with significant cation deficiency result in substantial overestimation of ferric iron contents (>10 wt%; Supplementary Data 2) to balance the negative charge of oxygen. Thus, stoichiometric and charge balance of 01JH analyses represent minimum and maximum ferric iron contents of Jack Hills detrital chromites, respectively.

Within-grain variability

Zoning. Although the largest systematic variations in chromite chemistry are between sample locations, line scans of 14WA and 16WA detrital chromites reveal distinct zonation trends (Fig. 8). Chromites do not exhibit morphologically or microstructurally distinct cores and rims, but we use those terms here to describe the centre and outer portions of grains. Most chromites have homogeneous ZnO contents (Fig. 8a) or slightly lower wt% ZnO towards rims (Fig. 8b and c). MnO is largely uniform across chromites, although slightly lower abundances towards the rim may be observed. Homogeneous Mg# appears to be restricted to chromites within high-ZnO 16WA7 (Fig. 8c), with all other samples yielding chromites that display distinct variability in Mg#. Low-ZnO samples, such as 14WA2 and 16WA5, yield clear decreases in Mg# from the core to rim of the grain (Fig. 8a). High-ZnO samples, such as 14WA3 and many examples within 14WA4, often yield

Table 1: Representative EPMA analysis of Jack Hills chromites

Sample:	14WA1	14WA2	14WA3	14WA4	16WA5	16WA6	16WA7	16WA8	16WA9	16WA10	01JH35	01JH36	01JH54
Grid ref. (UTM):	499135E 7105846N	499135E 7105846N	499135E 7105846N	499135E 7105846N	499135E 7105846N	499141E 7105855N	499102E 7105837N	499096E 7105837N	499395E 7106007N	499393E 7106004N	499772E 7106342N	499947E 7106431N	499137E 7105849N
Grain no.:	4	17	44	28	19	12	7	5 core	2	20	4	3	18
Rounding:	RO	RO (2)	RO	RO/RC	RO	EO	RO/EO	RO/RC	EO	RC			
SiO_2	0.02	0.08	0.00	0.00	0.01	0.01	0.00	0.01	0.03	0.03	0.03	0.15	0.11
TiO_2	0.18	0.32	0.27	0.09	0.12	0.19	0.28	0.08	0.22	0.04	0.54	0.25	0.53
Al_2O_3	18.52	11.89	18.13	18.53	20.28	18.26	22.43	19.02	19.48	20.35	21.16	22.37	15.98
Cr_2O_3	46.20	51.52	42.43	44.42	44.18	45.82	38.52	44.69	45.26	44.11	39.79	46.53	44.74
V_2O_3	0.12	0.19	0.16	0.11	n.a.	n.a.	n.a.	n.a.	0.14	0.13	0.23	0.20	0.17
Fe_2O_3	0.00	3.97	4.37	0.82	0.00	0.00	1.81	0.05	0.00	0.00	0.99	0.00	1.52
FeO	27.66	28.26	24.39	26.17	28.76	27.50	23.79	28.63	29.19	26.65	27.76	21.49	28.11
MgO	1.20	2.40	1.39	0.62	2.18	1.67	0.49	0.91	0.76	0.42	1.06	2.13	1.79
MnO	2.13	1.46	2.03	1.84	0.71	0.33	0.73	0.95	1.80	1.28	3.66	1.14	1.60
CaO	0.00	0.01	0.00	0.01	0.00	0.01	0.01	0.00	0.00	0.00	n.a.	n.a.	n.a.
Na_2O	0.00	0.10	0.00	0.00	n.a.	n.a.	n.a.	n.a.	n.a.	n.a.	n.a.	n.a.	n.a.
NiO	0.00	0.00	0.00	0.01	0.02	0.00	0.00	0.01	0.00	0.00	0.01	0.02	0.02
ZnO	3.08	0.84	7.29	6.19	2.11	4.32	11.24	3.95	1.39	5.50	2.22	3.70	1.65
CuO	n.a.	n.a.	n.a.	n.a.	n.a.	n.a.	n.a.	n.a.	n.a.	n.a.	0.01	0.00	0.02
Total	99.10	101.03	100.46	98.80	98.38	98.11	99.31	98.31	98.27	98.52	99.19*	100.07*	98.67*
Mg#	7.20	11.83	8.03	3.95	11.90	9.77	3.30	5.36	4.44	2.76	6.39	15.00	10.18
Cr#	62.60	74.41	61.09	61.66	59.37	62.74	53.53	61.19	60.92	59.25	55.78	58.26	65.26
$Fe^{3+}/\Sigma Fe$	0.00	11.22	13.87	2.74	0.00	0.00	6.42	0.00	0.00	0.00	3.12	0.00	4.63
$Fe^{3+}/\Sigma R^{3+}$	0.00	5.17	5.65	1.07	0.00	0.00	2.34	0.00	0.00	0.00	1.31	0.00	2.06

V_2O_3 not measured for 16WA5-7 and partial 16WA8. Fe_2O_3 calculated from AB_2O_4 stoichiometry using the equations of Droop (1987).
*Totals including oxygen; wt% O shown in Supplementary Data 2.

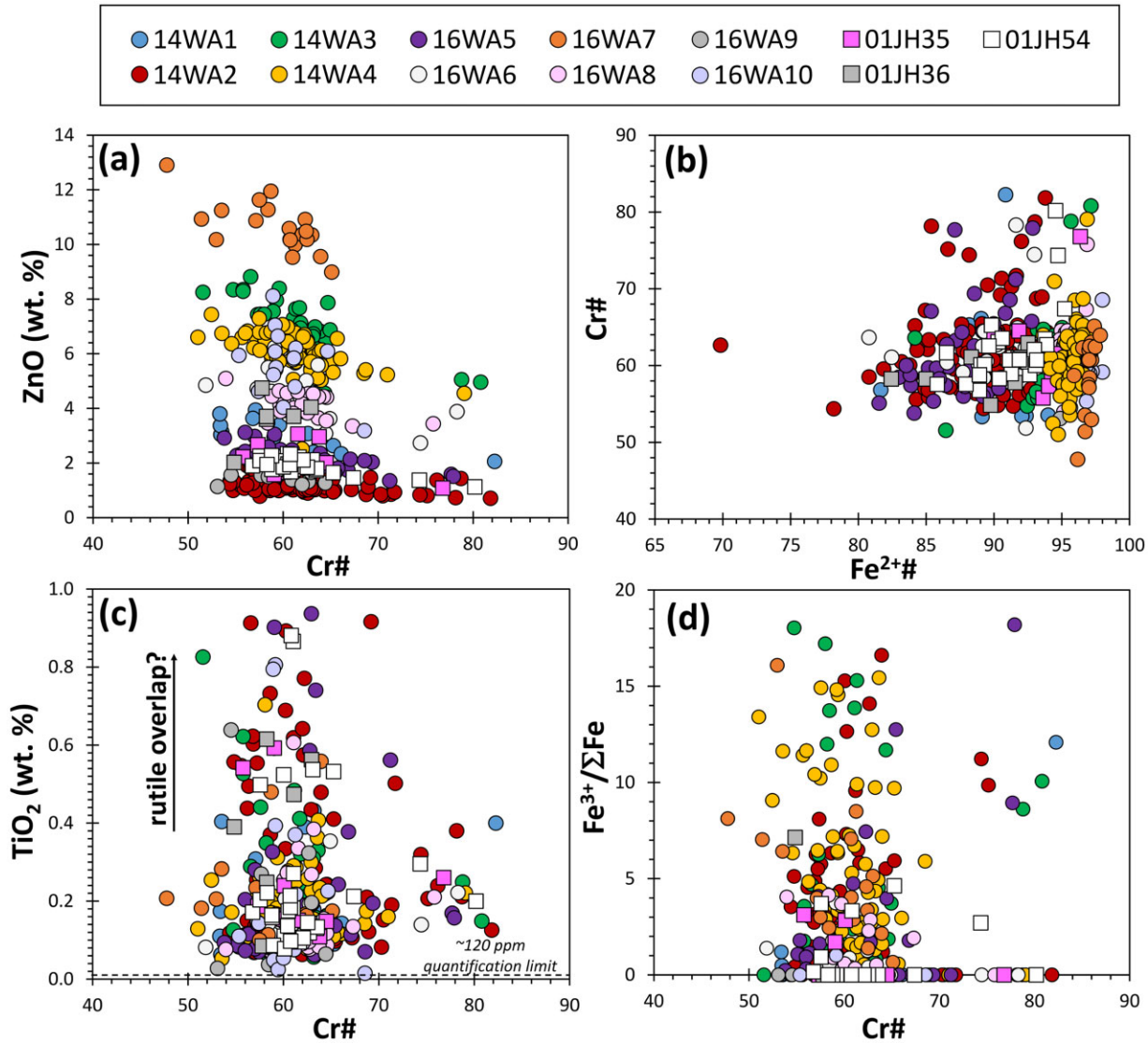

Fig. 7. Variation of Cr#. (a) ZnO vs Cr#. No variation in the range of Cr# despite apparent increasing ZnO. (b) Cr# vs Fe^{2+}# [100 × molar $Fe^{2+}/(Fe^{2+} + Mg^{2+})$]. (c) TiO_2 concentrations vs Cr#. Scatter towards 1 wt% a mixture of high-TiO_2 grains and likely overlap of rutile laths. High-Cr# grains appear to be slightly elevated in TiO_2 in comparison with bulk lower Cr# grains. (d) $Fe^{3+}/\Sigma Fe$ vs Cr#.

rims with higher Mg# (Fig. 8b) although lowering of Mg# from core to rim is also observed. Grains with elevated Mg# at the rims show increases in both MgO and FeO from core to rim, compensated by decreases in ZnO and MnO.

Whereas grains yield zoning profiles of divalent cations, intra-grain changes in Cr# are largely absent (Fig. 8). Core-to-rim trends of marginally higher or lower Cr# (e.g. ±2) are sometimes observed (Fig. 8a and c), but there is no systematic behaviour in samples from different locations. Like Cr#, Fe_2O_3 contents are generally homogeneous across chromite grains, with variability in some zonation profiles probably reflecting low calculated Fe_2O_3 contents. However, individual grains do yield distinct variations in Fe_2O_3 that appear systematic in origin, present as both decreases and enrichments in Fe_2O_3 from core to rim, with increasing Fe_2O_3 often coupled with a small increase in Cr# (Fig. 8a).

Coupled elemental and textural variation. Distinct zones of elevated Cr# within detrital chromite are present in a few samples (Fig. 9). These features are closely associated with pitted domains and fractures, and may exhibit diffuse or more commonly sharp boundaries with surrounding chromite (Fig. 9a–e). High-Cr# domains, also distinguished by an absence of fractures and inclusions in comparison with surrounding chromite (Fig. 9a and b), mostly occur at the edge of grains adjacent to enclosing fuchsite or associated with fractures (Fig. 9a–c). These domains may also be localized, occurring as distinct polygonal areas, apparently defined by crystallographic directions (Fig. 9d and e). These domains are characterized by high Cr# (>70), low totals (<98 wt%), the apparent absence of Fe_2O_3, lower ZnO and V_2O_3, and occasionally slightly elevated MnO. High-Cr# domains within detrital chromite are chemically indistinguishable from low-Fe_2O_3, high-Cr# grains

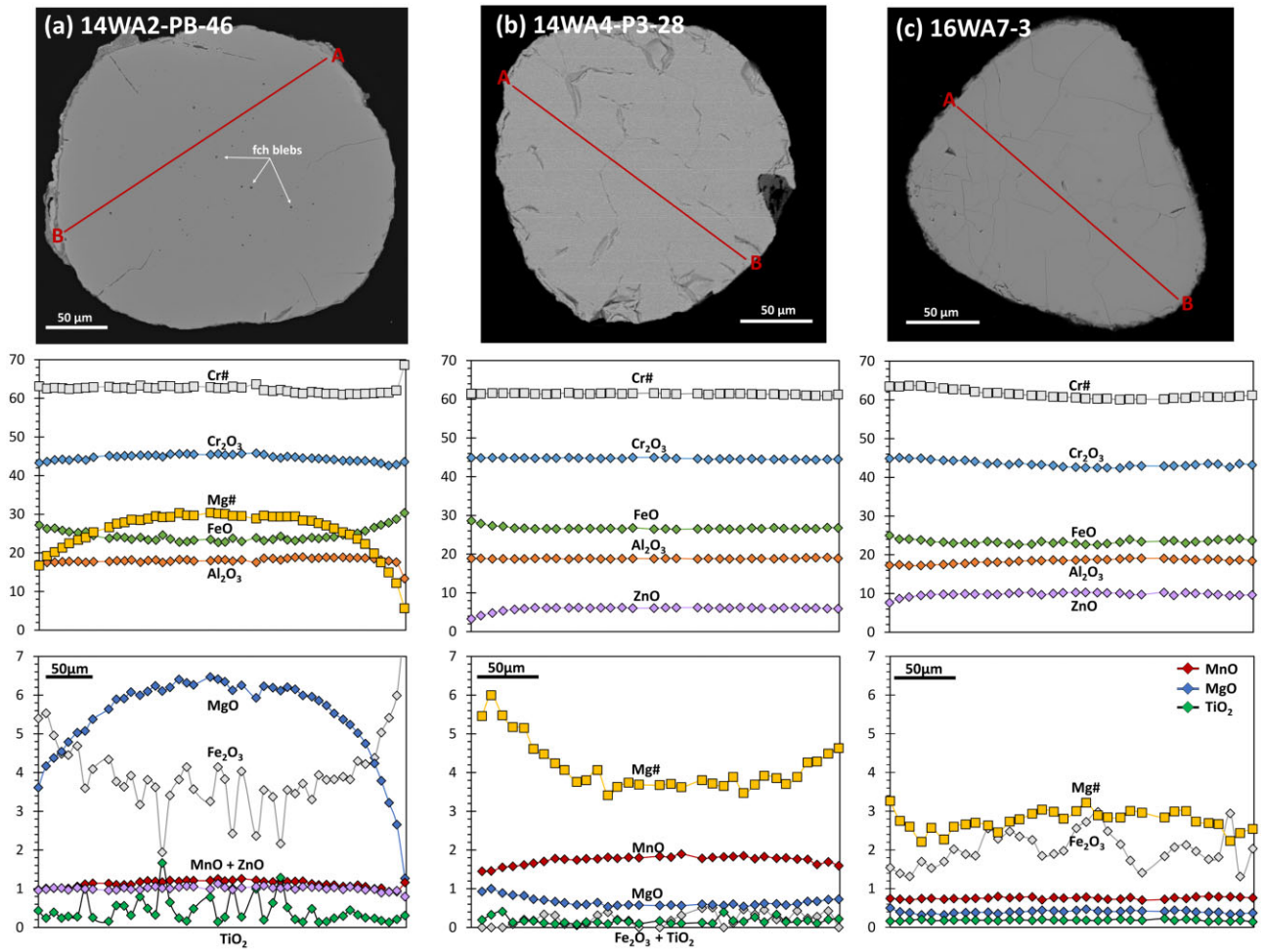

Fig. 8. Examples of zonation patterns observed within 14WA and 16WA Jack Hills detrital chromites, including BSE images of line path taken. Isolated, globular inclusions of fuchsite (Fch) also highlighted in 14WA2-PB-46. (a) Decreasing Mg# towards rims, most commonly shown by low-ZnO samples 14WA2 and 16WA5. 14WA2-PB-46 yields the most variable zoning patterns observed in all Jack Hills grains and is probably the least altered grain analysed. This example also includes elevated Fe_2O_3 at its rims, resulting in an area of slightly elevated Cr#. (b) Elevated Mg# towards rims, commonly observed in high-ZnO samples such as 14WA3-4 and 16WA7. ZnO and Mn are lost from chromite at the expense of FeO and MgO, increasing the Mg# of rims relative to the core of the grain. (c) Largely homogeneous Mg#. No change in mineral chemistry across the grain in divalent or trivalent cations; this example has a slight elevation in Mg# on one edge.

within the same samples. Only a single domain of low Cr# has been observed within chromite, bounding a monomineralic quartz inclusion alongside iron oxide (Fig. 9f).

Oxygen isotope compositions

Analysis of oxygen isotope ratio in various chromite size fractions was conducted to determine if detrital chromite grains preserve primary (magmatic) $\delta^{18}O$ values, or if there is evidence of oxygen exchange with the metasedimentary host rocks. Exchange of oxygen isotopes between chromite and surrounding quartz at low temperature (e.g. $<600\,^{\circ}C$) would result in lowered $\delta^{18}O$ values for chromite (Lowry *et al.*, 2003). Each sample showed $>1‰$ variability in $\delta^{18}O$, with $\delta^{18}O$ chromite values ranging from 0.03 to 2.19‰ (Fig. 10; Supplementary Data 1; Table 3). For samples 01JH36 and 01JH42, the lowest chromite $\delta^{18}O$ values (0.69 and 0.03‰, respectively) were detected in the smallest size fraction, and there was a systematic increase of $\delta^{18}O$ with grain size (Fig. 10a and b). In contrast, 01JH54 showed no systematic variation of chromite $\delta^{18}O$ with grain size, and also contained the highest $\delta^{18}O$ measured for chromite at 2.19‰ (Fig. 10; Supplementary Data 1; Table 3).

DISCUSSION

Chromite morphology and the origin of inclusion assemblages

The variably rounded morphologies of chromite, from RC to EO, attest to a protracted and complex reworking history of numerous detrital grains. Additionally, the presence of chromite within quartzite cobbles of metaconglomerates (Fig. 3b; Dare *et al.*, 2016) suggests

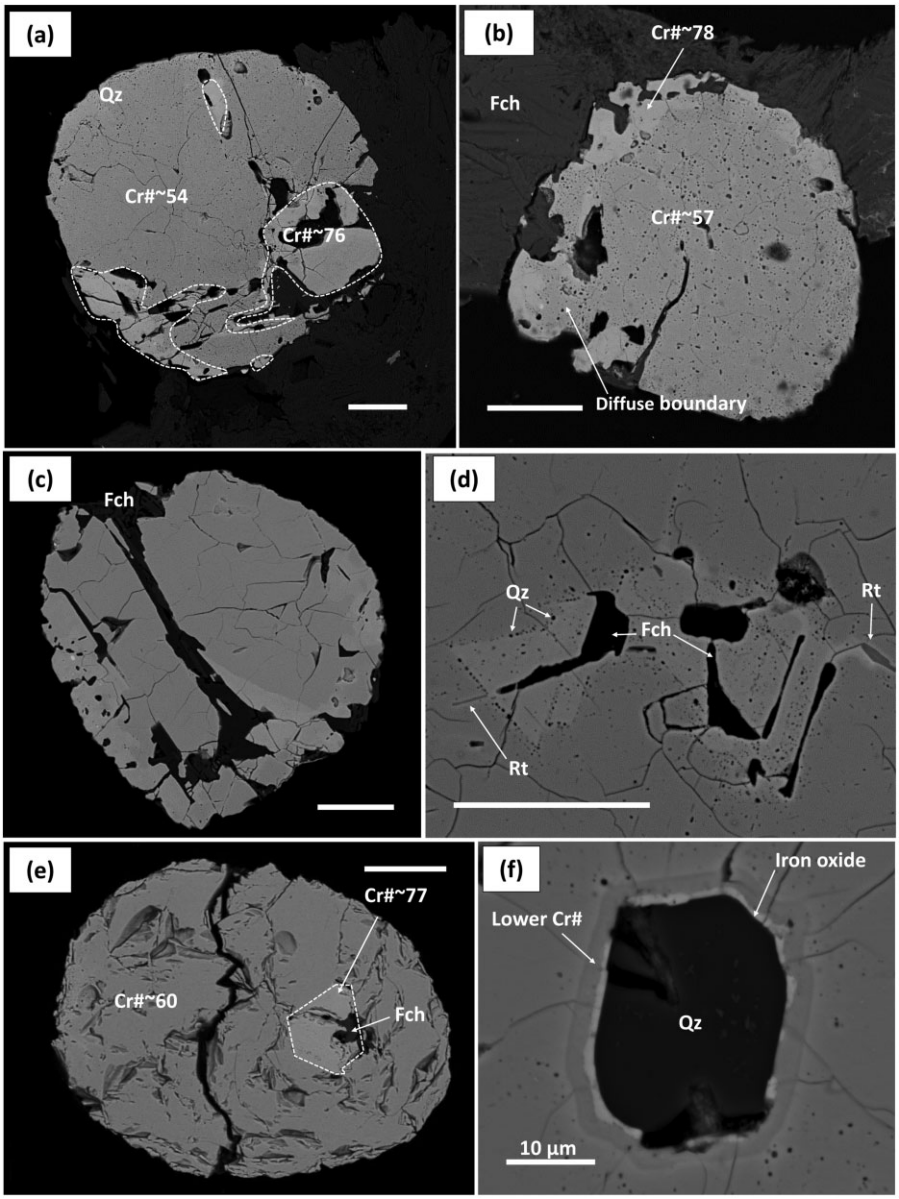

Fig. 9. Variation in mineral chemistry; BSE images with elevated contrast to highlight high-Cr# domains. (a, b) High-Cr#, pit-free domains at the edge of grains, and (c) along or associated with cracks. (d, e) High-Cr# domains bound by chromite crystallographic axes, closely associated with laths of fuchsite (Fch) and anhedral quartz (Qz) along margins of high-Cr# zones and rutile (Rt). (f) The only observed example of a domain of lowered Cr#, encircling an inclusion of quartz with iron oxide rims. (Note the radial fractures associated with the secondary inclusion.) Except where stated, all scale bars represent 50 μm.

cycling of some grains in at least two sedimentation events. Categorization of grains by shape may indicate provenance from multiple geographical sources or differing modes of sedimentary transport (Dott, 2003). The extensive sedimentary cycling history of some chromites is consistent with the mature nature of host metasedimentary rocks (>98 wt% SiO_2; Cavosie *et al.*, 2004) but at odds with the highly fractured nature of many grains (Fig. 4b and e), which would not survive extensive sedimentary transport. This strongly suggests that fracturing of grains occurred *in situ*, during deformation of the host metasedimentary rocks.

Jack Hills detrital chromites contain inclusion assemblages of quartz, fuchsite, rutile, Fe-oxide, monazite, and Fe-sulphide (Fig. 5). These phases, particularly quartz and fuchsite, typically form under distinctly different physical and chemical conditions compared with magmatic chromite. However, quartz and fuchsite are common components of Jack Hills quartzites and metaconglomerates, alongside minor secondary rutile, monazite and xenotime (Harrison *et al.*, 2007; Iizuka *et al.*, 2010; Rasmussen *et al.*, 2010). Inclusions of quartz and Cr-poor muscovite have also been reported within detrital zircon (Cavosie *et al.*, 2004; Hopkins *et al.*, 2008, 2010; Rasmussen *et al.*, 2011; Bell *et al.*, 2015*b*), as both monomineralic and polyphase inclusions alongside monazite and xenotime (Rasmussen *et al.*, 2011). Monazite and xenotime

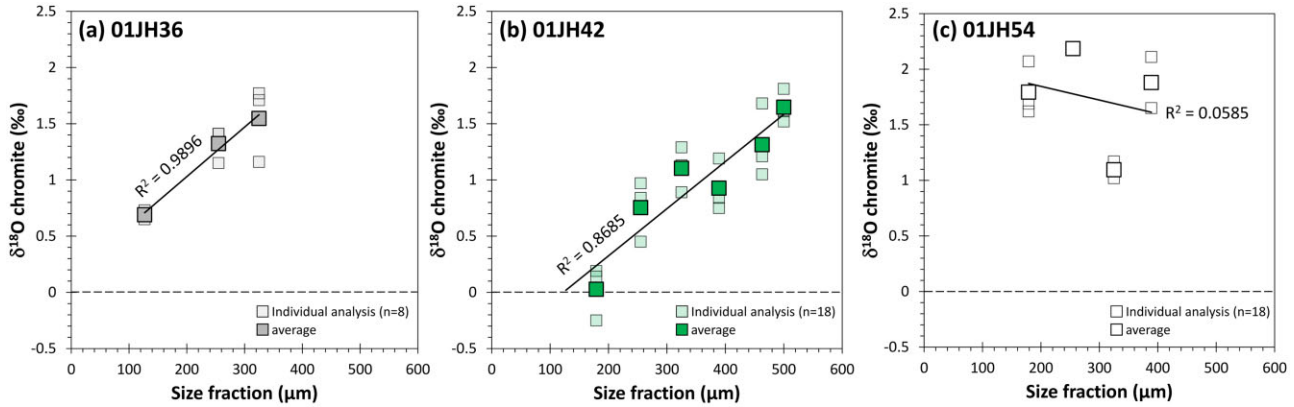

Fig. 10. Oxygen isotope ratios ($\delta^{18}O$ reported at ‰ variation to V-SMOW) for different size fractions of Jack Hills detrital chromite grains measured by laser fluorination. $\delta^{18}O$ uncertainties (2σ) are ±0.07 for 01JH36, ±0.11 for 01JH42 and ±0.07 for 01JH54. (a, b) Samples 01JH36 and 01JH42, which show strong evidence of grain size dependence on $\delta^{18}O$ values. (c) Sample 01JH54, showing no evidence of grain size dependence on $\delta^{18}O$ values.

inclusions within detrital zircons yield ^{207}Pb–^{206}Pb ages of ~2650 Ma and 800 Ma respectively that are demonstrably younger than the host grains (Rasmussen *et al.*, 2011), attesting to a secondary origin of many zircon inclusion assemblages. Additionally, Cameron *et al.* (2016) showed that ~60% of quartz inclusions within zircon exhibited evidence of $\delta^{18}O$ exchange with Jack Hills metasedimentary rocks. It is therefore hypothesized that many quartz inclusions within detrital zircons were significantly altered during metamorphism of host metasedimentary rocks or, alongside muscovite, rutile, monazite and xenotime, were precipitated from post-depositional fluids that filled voids left from the dissolution of primary apatite (Rasmussen *et al.*, 2011; Bell *et al.*, 2015*b*; Cavosie *et al.*, 2018; c.f. Hopkins *et al.*, 2010, 2012).

The occurrence of assemblages of the same phases as observed within detrital zircons, coupled with the unlikelihood of quartz and muscovite stability within the mafic–ultramafic melt that crystallized chromite, provides evidence that most inclusion assemblages within chromites are secondary in origin. Interestingly, many secondary inclusions of quartz and fuchsite are apparently isolated from visible fractures within chromites (Figs 5a and 8a). Isolation of inclusions has been used as a line of evidence for a primary origin of many quartz and muscovite inclusions within detrital zircons (Bell *et al.*, 2015*b*). The detection of clearly secondary, apparently isolated inclusion assemblages within detrital chromites suggests that caution should be applied when using this as a line of evidence for the presence of primary inclusions, and instead points to the presence of sub-micron or annealed fractures within grains, or fracturing below 2D surfaces shown by electron imaging (Cavosie *et al.*, 2018).

Our data therefore indicate that inclusion assemblages formed from interaction of detrital chromites and metamorphic fluids within the metasedimentary host. Pitted and porous domains, which are analogous to spongy textures described elsewhere (Gervilla *et al.*, 2012; Colás *et al.*, 2014) and host the same secondary mineral assemblages, were also probably formed by this process. Coarser, euhedral inclusions may reflect direct dissolution of primary inclusion phases, akin to aforementioned replacement of primary inclusion assemblages within detrital zircon (Rasmussen *et al.*, 2011). It is more problematic to prescribe an origin for inclusions of sulphide and rutile. Pyrrhotite and chromite are commonly co-liquidus phases under iron sulphide saturated magmatic conditions; however, secondary pyrite is often observed within Jack Hills metasedimentary rocks (e.g. Cavosie *et al.*, 2004; Supplementary Data 1) and iron sulphides (typically ≤40 μm pyrite, pyrrhotite, intergrowths of pyrite and pyrrhotite, and rarer pentlandite) are ubiquitous within isolated quartzite cobbles (Dare *et al.*, 2016). Pyrrhotite, pyrite and rare chalcopyrite inclusions within Jack Hills chromites appear to be closely linked to pitted domains (Fig. 5c). We therefore propose a secondary origin for Fe-sulphide inclusions within chromites.

Inclusions of rutile may be anhedral, globular or preserved as aligned laths, and are particularly abundant within pitted and porous domains. Observed alignment of exsolved or alteration phases within chromite (Figs 4e and 5a) is noted elsewhere, including in chlorite (Fleet *et al.*, 1993; Gervilla *et al.*, 2012) and phlogopite (Rollinson *et al.*, 2002). Whether rutile was precipitated from metamorphic fluids, or was exsolved from chromite, perhaps via changes in the oxidization state of grains (e.g. Cameron , 1979), is unclear. High-Ti domains associated with cracks within zircon (Harrison & Schmitt, 2007; Hofmann *et al.*, 2009), and the secondary growth of rutile within metasedimentary matrix (Harrison *et al.*, 2007), attest to Ti mobility within Jack Hills metasedimentary rocks. Although we consider a secondary origin of rutile most likely, we note that direct exsolution from chromite that previously had higher TiO_2 contents cannot be discounted.

Chromite mineral chemistry

Signatures of metamorphism

Jack Hills detrital chromites typically yield high ZnO and MnO coupled with low Mg# (≤30; Fig. 6). Chromites with such distinctive chemical compositions are uncommon and are largely attributed to secondary processes (e.g. Barnes, 2000). A number of studies have investigated the effects of secondary modification of chromite major, minor and trace elements (Barnes, 2000; González-Jiménez *et al.*, 2009; Mukherjee *et al.*, 2010, 2015; Gervilla *et al.*, 2012; Colás *et al.*, 2014). Various processes that modify chromite include the following: (1) elemental mobility via interaction with aqueous fluids during the breakdown of surrounding Mg–Fe silicates via serpentinization (Burkhard, 1993; Marques *et al.*, 2007; Hodel *et al.*, 2017) and/or metamorphism (Evans & Frost, 1975; Kimball , 1990 ; Barnes, 2000; González-Jiménez *et al.*, 2009; Gervilla *et al.*, 2012; Colás *et al.*, 2014; Fanlo *et al.*, 2015; Ahmed & Surour, 2016); (2) Cu–Zn–Ni– (Co) sulphide mineralization of the host rock (Wylie, 1987; Marques *et al.*, 2007; Fanlo *et al.*, 2015); (3) magmatic sulphide mineralization (Groves *et al.*, 1977). The effects of these processes on chromite chemistry are dependent on the temperature and longevity of alteration, the nature and fO_2 of the aqueous medium, the composition of the host rock and subsequent chromite/silicate ratio, and the fluid/rock ratio during modification (Colás *et al.*, 2014; Ahmed & Surour, 2016). The most commonly observed divalent cation mobility during thermal events is a decrease in Mg#, as Fe^{2+} diffusively enters the chromite lattice at the expense of Mg^{2+} (Barnes, 2000; Colás *et al.*, 2014). ZnO, MnO and, to a lesser extent, CoO also diffuse into the chromite lattice in exchange for MgO, NiO and often TiO_2 (Barnes, 2000; Colás *et al.*, 2014).

Within Jack Hills detrital chromites, coupled growth in ZnO content with increasingly homogenized and lowered Mg# probably signifies greater exchange with the modifying medium (Fig. 6a). This may indicate variable modification within their protolith; however, analogous signatures of alteration have been previously reported by Challis *et al.* (1995), where detrital chromites within fuchsitic sedimentary rocks yielded elevated ZnO (up to 13.7 wt%) and MnO (up to 3.5 wt%), coupled with low Mg#. Critically, the detrital grains described by Challis *et al.* (1995) possessed a well-constrained provenance, demonstrating that the observed signatures could only have formed during post-depositional metamorphism.

We propose that the dominant signatures of secondary modification within Jack Hills detrital chromites occurred from exchange of grains with metamorphic fluids and/or assemblages during metamorphism of their metasedimentary hosts. First, as established above, interaction of chromite with metamorphic fluids is shown by replacement of inclusion assemblages (Fig. 5) and the development of pitted and porous domains. Second, large differences in chromite chemistry between samples do not relate to the physical characteristics of grains, such as grain shape or size (Supplementary Data 1 Figs 9 and 10), but are a function of sampling site and therefore sedimentary horizon. Homogeneity of Mg# (e.g. 16WA7 and 16WA9; Fig. 6) requires modification under the same physicochemical conditions, including temperature, fO_2 and Mg# of modifying medium, despite variation in sedimentary transport characteristics. Observed Mg# uniformity is therefore difficult to reconcile with metamorphic modification within the original ultramafic or mafic protolith.

Finally, and most significantly, chromites yield intrasample homogeneneity yet substantial inter-sample chemical variability despite the proximity (often <5 m) of sampling locations (Fig. 2), with the meter-scale variability of ZnO and Mg# of detrital chromites reconciled by changes in grain size and modal proportions of chromite within the host metasedimentary rocks (14WA1-4; Supplementary Data 1). Chromites are the sole ZnO-bearing phase, but are mostly present at low modal proportions of <1 %. As such, minor changes in the modal proportion and grain size of detrital chromites can account for large variations of wt% ZnO within detrital chromites during interaction and exchange with secondary fluids. However, simple changes in the modal proportion of chromite cannot account for the observed wt% ZnO within 01JH36 chromites, which are present in discrete heavy mineral bands within which they represent a significant mineralogical component. Instead, 01JH36 chromite mineral chemistry may be reconciled by metamorphic equilibration of ZnO at length scales greater than heavy mineral bands (millimeter scale or greater) and, given the distance of this sample from the W-74 site (Fig. 2), variable physicochemical compositions of metamorphic fluids across the Jack Hills. Thus, variability in modification signatures may also reflect changing parameters of metamorphic fluids, as also suggested by the often poor correlation of Mg# and MnO with the modal proportion of detrital chromite.

Oxygen isotope compositions

In situ modification of chromites is also suggested by oxygen isotope compositions. The variation of $\delta^{18}O$ with grain size in chromites from samples 01JH36 and 01JH42 (Fig. 10a and b) indicates partial exchange of oxygen isotopes with the metasedimentary host rocks. If exchange was by diffusion inwards from the grain boundary, then greater modification of smaller grains is expected given their larger surface area to volume ratio. The lower $\delta^{18}O$ values of the smallest chromite grains from 01JH36 and 01JH42 may therefore approach equilibration with host quartz during metamorphism or retrogression. In contrast, chromite grains in sample 01JH54 show no grain size dependence on $\delta^{18}O$ (Fig. 10c). Given the conspicuously lower chromite $\delta^{18}O$ values recorded in 01JH35 and 01JH36 and preservation of Mg# zonation profiles within low-ZnO chromites, we tentatively interpret chromite $\delta^{18}O$ values in sample 01JH54 as pre-depositional. Low $\delta^{18}O$ (≤2.5–3.0 ‰) are

reported within chromitite from ophiolites and layered intrusions, and are thought to represent exchange with late-stage magmatic and sub-solidus fluids (Lowry *et al.*, 2003; Schannor *et al.*, 2018), or interaction with seawater during serpentinization (Mondal *et al.*, 2003). Lowered $\delta^{18}O$ within 01JH54 may therefore reflect pre-depositional alteration of chromite oxygen isotopes. However, if such modification occurred, exchange would appear to have occurred at conditions consistent with those experienced by Jack Hills metasedimentary rocks; thus, the processes associated with any pre-depositional alteration cannot be quantified.

Oxygen isotope ratios for the smallest chromite size fractions in samples 01JH36 and 01JH42 were compared with previously published $\delta^{18}O$ values for quartz in the same samples (Supplementary Data 1; Table 4; Cavosie *et al.*, 2005). Cavosie *et al.* (2005) found that values of $\delta^{18}O(Qz)$ are homogeneous at hand sample scale in these rocks, indicating metamorphic equilibration of quartz in pebbles and matrix. If attainment of oxygen isotope equilibrium between quartz and chromite is assumed, the $\Delta^{18}O$ value ($\Delta^{18}O_{Quartz-Chromite} = \delta^{18}O_Q - \delta^{18}O_C$) for samples 01JH36 ($\Delta^{18}O_{Q-C} = 12.02‰$) and 01JH42 ($\Delta^{18}O_{Q-C} = 12.70‰$), can be applied to calculate the temperature at which the observed fractionations were established (Zheng, 1991). Calculated temperatures are 412 °C and 390 °C for samples 01JH36 and 01JH42, respectively. Sample 01JH54 yields a distinctly smaller fractionation ($\Delta^{18}O_{Q-C} = 9.11‰$) that would correspond to a temperature of 530 °C if it represented metamorphic equilibration. However, as discussed above, the analysis of different-sized grains suggests that chromite grains in this sample preserve pre-depositional $\delta^{18}O$ and may not be appropriate for metamorphic thermometry. Although it cannot be demonstrated that oxygen isotope equilibrium was established between quartz and chromite based on $\delta^{18}O$ analysis of 2 mg aliquots in the other two samples, we note that the derived temperatures based on measured fractionations are consistent with greenschist facies metamorphic conditions previously documented within the Jack Hills (Cavosie *et al.*, 2004; Spaggiari *et al.*, 2007).

Quartz in the metasedimentary rocks analysed has been shown to have recrystallized during metamorphism, and yields homogeneous $\delta^{18}O$ values at greater than centimeter scales (Cavosie *et al.*, 2005). In contrast, chromites in the same samples preserve detrital morphologies, probably preserve gradients in $\delta^{18}O$ at sub-millimeter scale (Fig. 10), and thus are not equilibrated in $\delta^{18}O$. We therefore use the $\delta^{18}O$ values determined for quartz (Cavosie *et al.*, 2005) and temperatures determined from oxygen isotope thermometry to estimate the $\delta^{18}O$ value of fluids present during metamorphism (Supplementary Data1; Table 5). Calculated water $\delta^{18}O$ values using quartz–water fractionation factors of Sharp *et al.* (2016) and the published quartz $\delta^{18}O$ values yield water $\delta^{18}O$ values of 8.58‰ (at 412 °C) for sample 01JH42 and 8.16‰ (at 390 °C) for sample 01JH36; a value of water $\delta^{18}O$ of 8.50‰ (at 530 °C) for sample 01JH54 is comparable with those for the other two samples, but may be fortuitous given the lack of evidence for equilibration in sample 01JH54 (Fig. 10). Regardless, the range of all calculated water $\delta^{18}O$ values, from 8.2 to 8.6‰, is typical for magmatic or metamorphic fluids (Sheppard, 1986).

Trivalent cations: retained primary signatures?

Whereas divalent cations exchange more readily during metamorphism, trivalent cations appear largely immobile during low-temperature modification (e.g. Barnes, 2000). Chromite interacting with acidic fluids during sea-floor hydrothermal metasomatism may rarely induce trivalent cation exchange (Wylie *et al.*, 1987; Marques *et al.*, 2007; Hodel *et al.*, 2017); more generally, however, nascent trivalent mobility occurs at greenschist facies metamorphism (Kimball *et al.*, 1990; González-Jiménez *et al.*, 2009) and becomes increasingly pervasive at and above amphibolite facies (Barnes, 2000; González-Jiménez *et al.*, 2009; Colás *et al.*, 2014). Under oxidizing conditions, trivalent cation exchange most commonly facilitates the transition of chromite to ferritchromit [$Fe^{2+}(Fe^{3+},Cr)_2O_4$], where Al_2O_3 is lost to Fe_2O_3 either diffusively (Wylie *et al.*, 1987; Gervilla *et al.*, 2012; Colás *et al.*, 2014) or via reaction with magnetite rims (Evans & Frost, 1975; Barnes, 2000). Extensive formation of ferritchromit and Cr-magnetite, and thus modification of chromite core compositions, appears to be largely restricted to amphibolite facies metamorphism and above (Barnes, 2000).

Regardless of the degree of secondary modification of divalent cations, Jack Hills detrital chromites possess a broad but consistent range in Cr# across all metasedimentary sample locations (Fig. 7). The range of Cr# may be explained by either the absence of significant trivalent mobility or the equilibration of chromite during secondary modification with a Cr–Al-bearing equilibrant (e.g. fuchsite or metamorphic fluid). If secondary exchange was significant for trivalent cations, homogenization to lower or higher Cr# in increasingly Zn-rich samples should have occurred. This is not observed. Additionally, zonation profiles of variable Mg# but homogeneous Cr# within low-ZnO chromites (Fig. 8a) would require more exchange, and thus faster diffusion, of trivalent than divalent cations. Such an order of relative diffusivities is in strong contrast to previous literature (e.g. Barnes, 2000), and is considered extremely unlikely.

Unmodified Cr# within chromites is at apparent odds with the presence of surrounding fuchsite, whose elevated Cr content is almost certainly derived from detrital chromites. Fuchsite has Cr_2O_3 concentrations of ~2–3 wt% (Cr# <5; Supplementary Data Table 6), which decrease with increasing distance from detrital chromite grains (e.g. Rasmussen *et al.*, 2011). Such low concentrations within fuchsite require only minor mobilization of Cr from chromite, and suggest that the

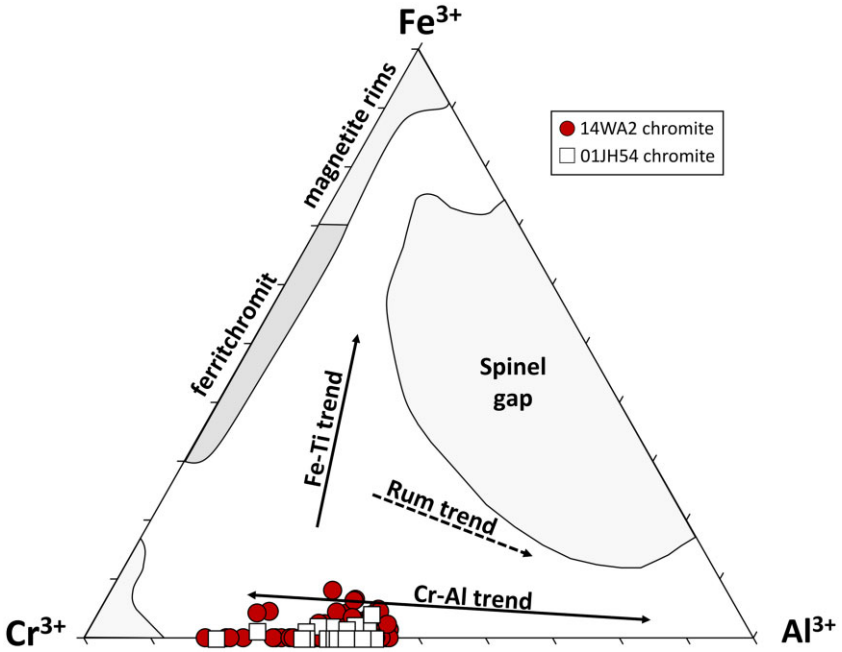

Fig. 11. Cr^{3+}–Al^{3+}–Fe^{3+} trivariant plot, modified from Barnes & Roeder (2001), showing three magmatic compositional pathways for spinel: Cr–Al, Fe–Ti, and Rum trends. The compositional space of ferritchromit, Cr-magnetite, and spinel miscibility gaps are shown for reference. Core or near core compositions of low-ZnO 14WA2 and 01JH54 chromites are plotted.

Cr required was scavenged from more heavily altered areas of chromite during metamorphic precipitation of fuchsite, or from dissolution of grains in acidic fluids. This is supported by lobate boundaries of detrital chromites with surrounding fuchsite (Fig. 9a and b). Selection of grains with well-defined shapes has probably filtered our dataset for such heavily modified compositions; the process of fuchsite formation causes ragged grain boundaries and extensive fracturing of chromites, which significantly modifies grain morphology (Fig. 3).

Importantly, sharp boundaries indicate negligible diffusion between high-Cr# domains and bulk chromites (Fig. 9). Whereas the association of high-Cr# domains with fuchsite and pitted domains indicates that they represent areas of elevated alteration, widespread diffusion of trivalent cations would overprint sharp boundaries, inducing gradients in both zonation profiles and BSE images. High-Cr# domains therefore provide strong evidence for inhibited trivalent mobility. High-Cr#, low-Fe^{3+}# and inclusion-free zones of alteration have previously been documented by Arai *et al.* (2006), with the distinct boundaries between the bulk chromite and high-Cr# domains suggested to represent a spinel miscibility gap at high-Cr, low-Fe^{3+} conditions (not shown in Fig. 11). The exact mechanism of formation for high-Cr# domains remains unclear; Arai *et al.* (2006) argued that such domains represent the loss of Al^{3+} without concurrent addition of Fe^{3+}. Alternatively, high-Cr# domains may reflect non-stoichiometric compositions transitional to ferritchromit or fluid-mediated recrystallization, although further microstructural analysis would be required to show this.

High-Cr# domains yield strong compositional similarities to high-Cr# chromite, which creates increased uncertainty as to the primary origin of high-Cr# grains. However, inter-grain variability in Mg# is still apparent within 14WA2, and the zonation profile of high-Cr# 14WA2-PB-12 (Cr# ~75) shows Mg# variability (Supplementary Data 1 Fig. 11). If elevated Cr# were a product of enhanced trivalent mobility, Mg# heterogeneity should not be observed. Mg# heterogeneity, coupled with the sharp boundaries of high-Cr# domains, therefore provides strong evidence that chromite grains with consistently high and homogeneous Cr# are pre-depositional in origin.

Timing and cause of chromite modification

It is apparent from the mineral chemistry and inclusion assemblages of Jack Hills detrital chromites that all grains were modified within host metasedimentary rocks. However, the timing and magnitude of metamorphic events within the Jack Hills are poorly understood (e.g. Kemp *et al.*, 2018). Previous work has attested to three thermal or fluid flow events within Jack Hills metasedimentary rocks, at ~2650, ~1850–1800 and 800 Ma (Spaggiari, 2007; Rasmussen *et al.*, 2010, 2011; Kemp *et al.*, 2018).

Dominant metamorphic signatures; an ~2650 Ma event

Metamorphism at ~2650 Ma has been proposed to represent peak metamorphic conditions at the W-74 site (Rasmussen *et al.*, 2010, 2011). Although inclusion assemblages within Jack Hills chromites have not been dated, and so cannot be definitively linked to this event,

previous investigation of secondary monazite and xenotime within detrital zircons from the W-74 site showed a large population of this age (Rasmussen *et al.*, 2011). Monazite–xenotime Gd exchange and Ti-in-quartz thermometry indicate metamorphic temperatures of <487 °C (Rasmussen *et al.*, 2011), suggesting upper greenschist facies metamorphism. Importantly, temperatures calculated here for oxygen isotope equilibrium between chromite and quartz fall within the range of temperatures anticipated for greenschist facies metamorphism, and may therefore support metamorphic modification of chromite at this time. As the ~2650 Ma event represents the highest grade of metamorphism experienced by association 3 metasedimentary rocks, this event probably imposed the observed chromite mineral chemistry. The chemical compositions of Jack Hills chromites can therefore be explained by partial to complete exchange with Fe-, Zn- and Mn-bearing metamorphic fluids and mineral assemblages during upper greenschist to lower amphibolite facies metamorphism at *c.* 2650 Ma. Metamorphic fluids were probably acidic to facilitate the mobility of Ti^{4+} (e.g. Van Baalen, 1993), and allow localized dissolution of chromite to form fuchsite.

This event also coincides with amphibolite to granulite facies metamorphism throughout the Narryer Terrane, including gneisses adjacent to the belt, and ubiquitous granitic emplacement within the entire Yilgarn Craton (Kemp *et al.*, 2018). Granite emplacement includes the *c.* 2650 Ma monzogranite ('The Blob granite'; Pidgeon & Wilde, 1998), which intrudes the Jack Hills belt to the SW of Erawondoo Hill (Fig. 2a). Speculatively, this intrusion, or other granitic intrusions adjacent to the Jack Hills belt, may have supplied heat and a metasomatic component (particularly Zn) to metamorphic fluids; similarly modified detrital chromites reported by Challis *et al.* (1995) were postulated to have gained their chemical compositions by interaction with fluids derived from local granitic plutons. An alternative and more local source of Zn within Jack Hills metasedimentary rocks may come from dissolution of sphalerite (ZnS), which may be a potential detrital phase given the abundance of Fe-sulphides within quartzite cobbles.

Studies have shown that metasedimentary rocks with Proterozoic depositional ages are complexly intercalated with and at the same apparent metamorphic grade as metasedimentary associations with inferred Archean depositional ages (Cavosie *et al.*, 2004; Dunn *et al.*, 2005; Grange *et al.*, 2010; Wang & Wilde, 2018). This intercalation, coupled with ~1850–1800 and ~800 Ma ages within the Jack Hills (Spaggiari *et al.*, 2007; Rasmussen *et al.*, 2010, 2011), indicates Proterozoic overprinting at a lower metamorphic grade than peak metamorphic conditions. Subtle zonation trends within some chromites, namely increased Mg# within 14WA4 (Fig. 8b), may be reconciled by minor elemental mobility (Mg, Fe, Zn) within the Proterozoic.

Pre-depositional modification?

Given the susceptibility of chromite to sub-solidus exchange, signatures of modification prior to deposition must also be considered. Divalent cations have undergone significant exchange within host metasedimentary rocks; it is unclear if preservation of high Mg# within the cores of some low ZnO grains (e.g. 14WA2-PB-46; Fig. 6b) represent pre-depositional Mg# or have undergone partial exchange. However, pre-depositional metamorphism of accessory chromites (i.e. within their protolith), should result in trivalent cation mobility in the form of development of ferritchromit rims (Barnes, 2000; Colás *et al.*, 2014). While the generation of ferritchromit is limited within chromitites, where the higher modal abundance of chromite in chromitite has been shown to inhibit significant metamorphic exchange and thus the generation of ferritchromit (e.g. Mukherjee *et al.*, 2010), chromitite typically represents relatively minor components of igneous bodies (Barnes & Roeder, 2001). Given the presence of EO, which have undergone little abrasion and rounding during sedimentary reworking, ferritchromit or magnetite rims should be clearly visible if present prior to deposition. No ferritchromit (rims or otherwise) has been observed within this study, providing evidence chromites have not undergone resolvable trivalent mobility prior to erosion from their protoliths. While we cannot definitively exclude trivalent cation mobility prior to deposition, we suggest that Cr# of Jack Hills detrital chromites represent the most robust chemical signature for investigation of provenance.

Provenance

Even with the protracted metamorphic histories seen in detrital chromites, some chemical signatures place constraints on their provenance. Consistent variability of Cr#, regardless of grain shape, may indicate a common mafic or ultramafic protolith. Although we base this interpretation on least altered chromites within samples 14WA2 and 01JH54, the consistent range of chromite Cr# regardless of rounding shape from all 14WA, 16WA and 01JH metasedimentary rocks potentially suggests that a single, large-scale magmatic source potentially dominated the mafic and ultramafic crust within the catchment of the Jack Hills sedimentary rocks. Unfortunately, important chemical tools for understanding the petrogenesis of chromite and consequently their protolith, namely Mg# and TiO_2, are not appropriate to apply to Jack Hills detrital chromites owing to modification within host metasedimentary rocks. We propose that trivalent cation mobility was limited within Jack Hills detrital chromites, but cannot fully exclude metamorphic re-equilibration of $Fe^{3+}/\Sigma R^{3+}$ prior to deposition. Given these uncertainties, as well as chromite non-stoichiometry and the presence of rutile laths, measured $Fe^{3+}/\Sigma R^{3+}$ and TiO_2 contents represent minimum values. The retention of unmodified Cr# within

cores of Jack Hills chromite will therefore yield the most information on provenance of detrital grains.

To gain understanding of the petrogenesis of Jack Hills detrital chromites, and potentially of mafic and ultramafic crust within the Narryer Terrane, we use the fields of Barnes & Roeder (2001), which were determined in a comparative study of over 26 000 spinels from different tectonic settings. We compare these fields with grains from 14WA2 and 01JH54, which, owing to low ZnO coupled with partial exchange of Mg#, we interpret to represent the least altered detrital chromite compositions. The chemical compositions of chromitites within the fields of Figs 10–13 are excluded, as chromitites compromise a low volumetric component of igneous bodies, particularly layered intrusions, and have been suggested to induce bias within provenance studies (Power *et al.*, 2000; Barnes & Roeder, 2001). Although Jack Hills detrital chromites appear to conform to a Cr–Al trend (Fig. 11; Irvine, 1967; Barnes & Roeder, 2001), where no enrichment of Fe^{3+} is observed with changing Cr#, this probably reflects non-stoichiometry. The consistently low ferric iron contents of chromites are not suggestive of Fe–Ti or Rum trends (Fig. 11), which form via the reaction of plutonic chromites with intercumulus liquid enriched in both Fe^{3+} and Ti.

As expected, in Cr# vs Fe^{2+}# (inverse Mg#) compositional space, Jack Hills detrital chromites fall within the 90th percentile of spinel within high-grade metamorphic rocks (Fig. 12a). The decrease of Mg# within Jack Hills detrital chromites owing to metamorphic exchange results in Mg# comparable with that of chromites modified within mafic–ultramafic protoliths; this process is also shown in Fig. 12d, where an increase in metamorphic grade from greenschist to amphibolite facies results in significantly lowered and homogenized Mg# within komatiitic chromites. Although Jack Hills detrital chromites yield a superficially similar Cr# variability to those modified by metamorphism, the range in Cr# shown within the metamorphic field (Fig. 12a) represents compositions transitional from magmatic Cr# to ferritchromit and magnetite. As such alteration phases are absent within Jack Hills chromites, and zonation profiles show limited Cr# variability, this process cannot explain the fit of grains to the metamorphic field of Barnes & Roeder (2001). A different provenance is therefore required for the observed Cr#.

The variable and moderate to high Cr# values of Jack Hills detrital chromites (typically 55–70) are comparable with those of ophiolitic chromites (Fig. 12b), continental layered intrusions (Fig. 12c), and intra-plate settings such as ocean-island tholeiites and oceanic plateaux (Dick & Bullen, 1984; Barnes & Roeder, 2001; Arai *et al.*, 2011). Critically, the Cr# values of Jack Hills chromites indicate that the majority of detrital grains cannot be derived from komatiites (Fig. 12d). As a product of high-temperature and high-degree mantle melts, komatiites have high Cr/Al ratios and therefore yield chromite with clustered and high Cr# (typically >70; Barnes & Roeder, 2001). In comparison with both Al-undepleted komatiites (AUDK; Fig. 12d) and Al-depleted komatiites (ADK), Jack Hills detrital chromites yield more variable and moderate Cr# (typically 55–70). ADK are not shown in Fig. 12 as they yield chromite with too high Cr# (>85) to represent a source of Jack Hills detrital chromites. Some portions of komatiitic lavas, such as olivine-rich dunitic channels and sheets, have been shown to yield chromite with lower Cr# (60–75) than bulk ADK and AUDK (Barnes, 1998; Barnes & Roeder, 2001). For example, a recent study of detrital chromite in fuchsitic quartzites of the Central Slave Cover Group argued for an origin from komatiitic dunite, in part owing to moderate Cr# of 58–70 (average Cr# 64; Haugaard *et al.*, 2021). However, detrital chromite purportedly sourced from komatiites in Witwatersrand conglomerates (Barnes & Roeder, 2001) and the Green Sandstone Bed in the Barberton greenstone belt (Lowe *et al.*, 2021) show a distinct distribution in Cr#, with a peak at Cr# ~80 that tails strongly towards lower Cr# compositions. This Cr# distribution may reflect a lower overall proportion of chromite within reduced dunites or preferential loss of chromite with poikilitic or dendritic morphologies, which are abundant in komatiitic dunite bodies (Barnes, 1998; Godel *et al.*, 2013). Komatiitic chromite with more moderate Cr# (<70) would therefore be unlikely to dominate the detrital chromite record over high-Cr# (>70) counterparts, arguing strongly against derivation of most Jack Hills detrital chromites from a komatiitic source.

We suggest that, on the basis of Cr#, the most likely provenance of Jack Hills detrital chromites is one or more layered intrusions. Notably, although chromitite fields are not included in Figs 12 and 13, Jack Hills detrital chromites yield Cr# comparable with those of Stillwater 'G' and Bushveld chromitites (e.g. Campbell & Murck, 1993; Langa *et al.*, 2020, and references therein). Although variable chromite morphologies may reflect different transport mechanisms, an absence of chemical variation with rounding shape of grains may be further qualitative evidence of a potential layered intrusion source; layered intrusions may yield consistent lithologies and mineral chemistry laterally for many kilometres. In the absence of definitive Fe_2O_3 or TiO_2 concentrations, tectonic settings with comparable Cr#, including podiform and other mantle-derived Cr-spinel, cannot be excluded (as shown by ophiolites; Fig. 13a).

However, chromite from early Archean anorthositic layered intrusions yields marked physicochemical differences from those from stratiform complexes, which dominate the layered intrusion fields of Figs 12 and 13. Archean anorthositic layered intrusions typically form sill-like bodies that are thought to represent subvolcanic, conduit-type intrusions coeval to overlying greenstone belts; they host discrete anorthositic layers and are of significantly lower volume than Proterozoic massif-type anorthositic intrusions. Archean sill-like anorthositic intrusions yield spinel grains that are typically Fe-rich, with populations of high Cr# (>70) and/or

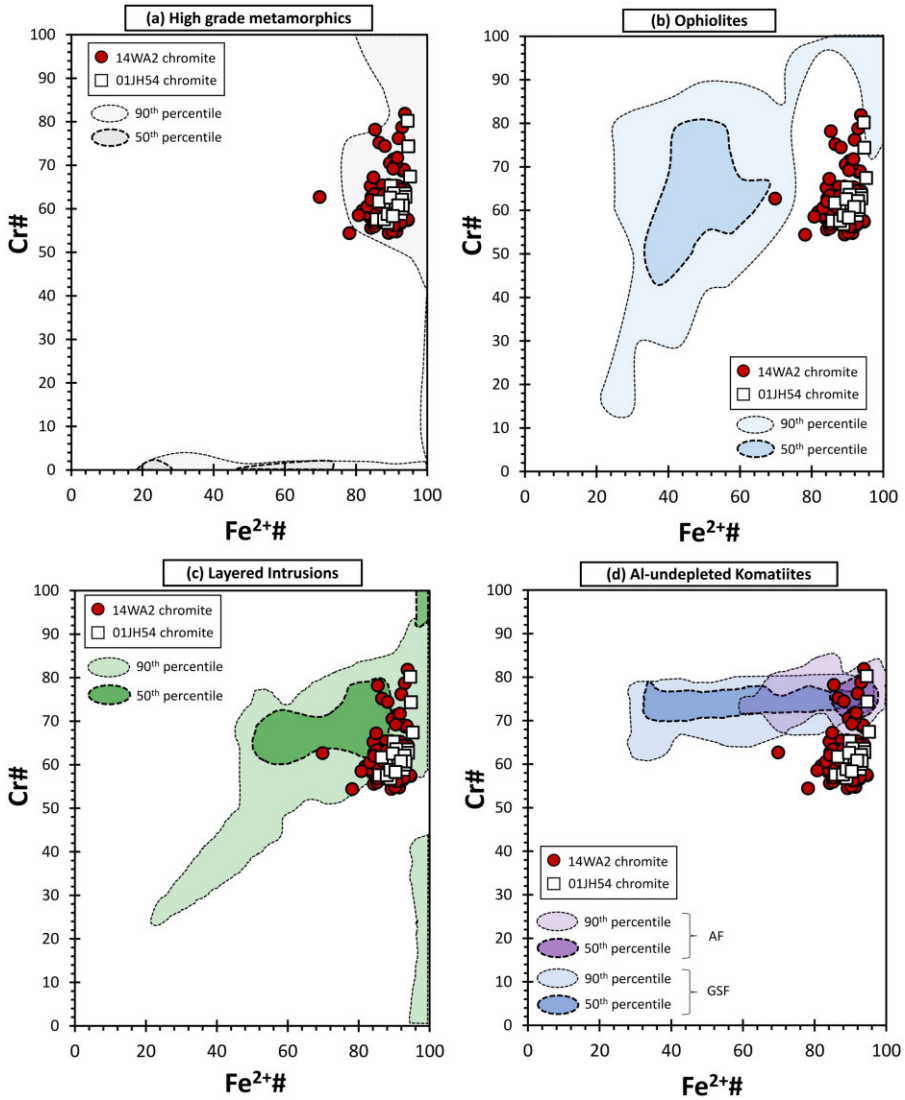

Fig. 12. Provenance: Cr# vs Fe^{2+}# [100 × Fe^{2+}/(Fe^{2+} + Mg^{2+})], diagrams modified from Barnes & Roeder (2001). (a) Strong fit of 14WA2 detrital chromite with chromite that has undergone high-grade metamorphism owing to exchange of Mg^{2+} for Fe^{2+}, and thus increased Fe^{2+}#. (b) Fit of bulk field for chromite from ophiolites, although Jack Hills chromites plot at considerably higher Fe^{2+}# owing to metamorphic exchange of Mg^{2+} for Fe^{2+}. (c) Strong fit of chromite Cr# in Jack Hills chromite with chromite from continental layered mafic intrusions. Jack Hills detrital chromite Fe^{2+}# values are again generally higher than 50th percentile owing to metamorphic exchange. (d) Distinct absence of fit with chromite from Al-undepleted (AUD) komatiites. GSF, greenschist facies AUD komatiites; AF, amphibolite facies AUD komatiites.

low Cr# (<50) (Rollinson *et al.*, 2002, 2010; Mondal *et al.*, 2006; Dharma Rao *et al.*, 2013; Mukherjee *et al.*, 2015; Rowe & Kemp, 2020), thought to reflect derivation from parental melts of komatiitic, boninitic or hydrous basaltic compositions (Ashwal and Bybee, 2017). Thus, typical mineral chemistry of anorthositic layered intrusive chromites is not comparable with that of Jack Hills chromites. Although chromites extending to Cr# comparable with that Jack Hills detrital chromites are documented (e.g. Mukherjee *et al.*, 2010), they typically represent a minor component of bulk chromite compositions. As with chromites from komatiitic dunitic channels, such chromites are unlikely to dominate detrital records over higher Cr# counterparts.

Although Jack Hills detrital chromites do not yield Cr# equivalent to Cr-spinel from sill-like Archean anorthositic layered intrusions, chromites from late Archean layered intrusions with comparable chemical compositions are known (e.g. Rollinson *et al.*, 2010; Berger *et al.*, 2013; Szilas *et al.*, 2018). The development of massif-type anorthositic intrusions at the beginning of the Proterozoic are thought to coincide with the emergence of increasingly thickened and strengthened lithosphere, a consequence of secular cooling and potentially shifting geodynamic regimes (Ashwal & Bybee, 2017). This therefore does not exclude the presence of similar layered intrusions during the early Archean; the preservation potential of larger, and thus higher density,

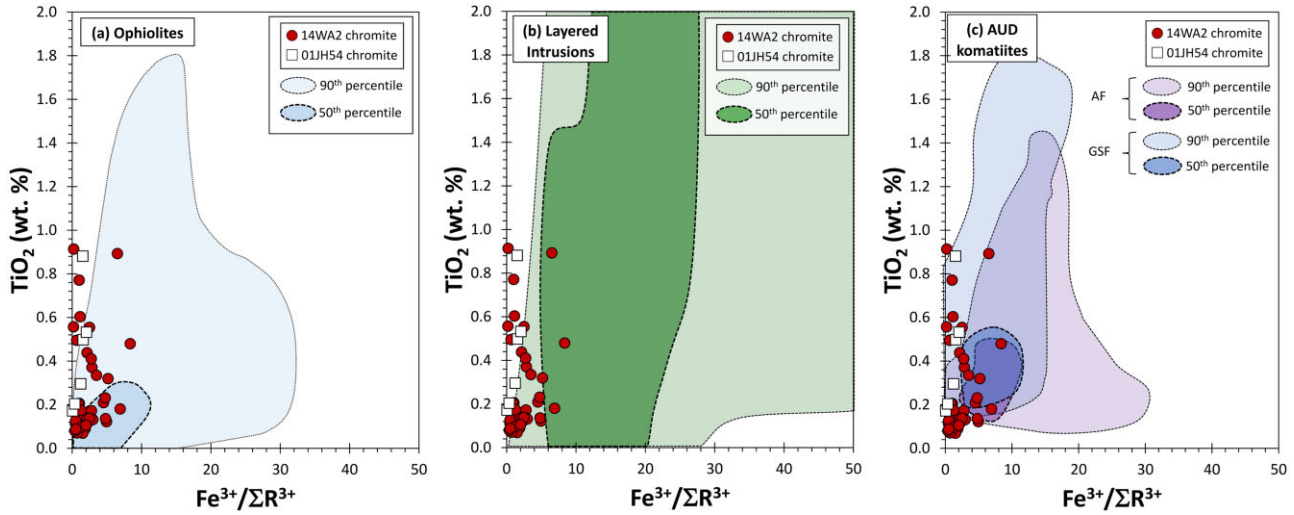

Fig. 13. Provenance: TiO_2 vs $Fe^{3+}/\Sigma R^{3+}$, diagrams modified from Barnes & Roeder (2001). Chromites that yield unmistakably non-stoichiometric compositions (i.e. cation totals less than three after normalization to four oxygens) are excluded for clarity. Fit of 14WA2 and 01JH54 chromite to all fields and for (a) ophiolites, (b) layered intrusions and (c) Al-undepleted komatiites (AUD). GSF, greenschist facies AUD komatiites; AF, amphibolite facies AUD komatiites.

stratiform intrusions would be significantly lower in the presence of hotter Archean mantle.

Potential sources within the Narryer Terrane

As the mineral chemistry of Jack Hills detrital chromites alludes to a layered intrusion origin, and unpublished Re–Os isotopic data yield model ages that are at least Palaeoarchean in age (Valley *et al.*, 2005), the sole described layered intrusion within the Narryer Terrane, the 3730 Ma Manfred Complex (Fletcher *et al.*, 1988; Kinny *et al.*, 1988; Myers, 1988b; Rowe & Kemp, 2020), can be considered as a potential source. Spinel within the Manfred Complex is dominantly spinel *sensu stricto* or picotite, and occurs closely associated with magmatic olivine (Rowe & Kemp, 2020), or exsolved from cumulus orthopyroxene or clinopyroxene. Chromite is completely absent in Manfred Complex harzburgites and websterites studied by Rowe & Kemp (2020); however, metaperidotites within the Manfred Complex do contain chromite (Fletcher *et al.*, 1988; Myers, 1988b; Kemp *et al.*, 2018). Below we compare the least altered 14WA2 and 01JH54 detrital grains with chromites from Manfred Complex sample 13TKN22 (Supplementary Data 1), a pyroxene-phyric peridotite metamorphically modified to hornblende and altered to serpentine.

Chromites from 13TKN22 ($n = 13$ analyses) occur as disseminated crystals with variably formed magnetite rims (Fig. 14a and b), and yield consistent Cr# of 76–80 (Table 2), coupled with low Mg# of <20, probably reflecting metamorphism of the host metaperidotite. These chromites yield limited ZnO (average 0.6 wt%) and heterogeneous MnO (0.4–1.4 wt%). NiO is present at magmatic concentrations of >0.1 wt%, but this may reflect the high magnetite component of 13TKN22 chromites (Barnes, 1998). Although divalent cation mineral chemistry suggests metamorphic alteration of 13TKN22 chromites, the sharpness of the boundary between chromite cores and magnetite rims (Fig. 14a and b) and the tightly clustered compositions of cores (Fig. 14d and e) indicate restricted trivalent element mobility (e.g. Barnes, 2000). Whereas the highest Cr# Jack Hills detrital grains overlap with the Cr# of 13TKN22 chromites (Fig. 14), detrital chromites possess significantly lower ferric iron contents and TiO_2, although given the uncertainties introduced by Ti mobility within host metasedimentary rocks comparisons should be taken tentatively. Chromites from 13TKN22 therefore cannot account for the bulk population of Jack Hills chromite detrital grains, which possess lower Cr#, and these lithologies did not represent the dominant component of mafic to ultramafic crust within the erosional catchment of Jack Hills metasedimentary rocks.

Although historically mafic and ultramafic crust within the Narryer Terrane tends to be collectively grouped as the Manfred Complex, more recent geochronological investigations have shown that many of these lithologies actually have Paleoarchean igneous crystallization ages (Kemp *et al.*, 2018). Continued investigation of these units may reveal further insights into the provenance of Jack Hills detrital chromites. Mafic and ultramafic rocks that occur within the Jack Hills belt may also represent the source for Jack Hills detrital chromites, particularly given the proximal source suggested for EO. Jack Hills mafic and ultramafic rocks are heavily sheared and extensively recrystallized (Spaggiari, 2007); however, analysis of one sample (16WA13; Supplementary Data 1) found relict chromite cores within texturally distinct chromite stringers. Whether this texture is igneous or a product of deformation is unclear, but the development of thick and indistinct magnetite and ferritchromit rims (Fig. 14c and d) records evidence for at least amphibolite facies metamorphism (e.g. Barnes, 2000), probably representing amphibolites facies metamorphism of the Jack Hills belt prior to

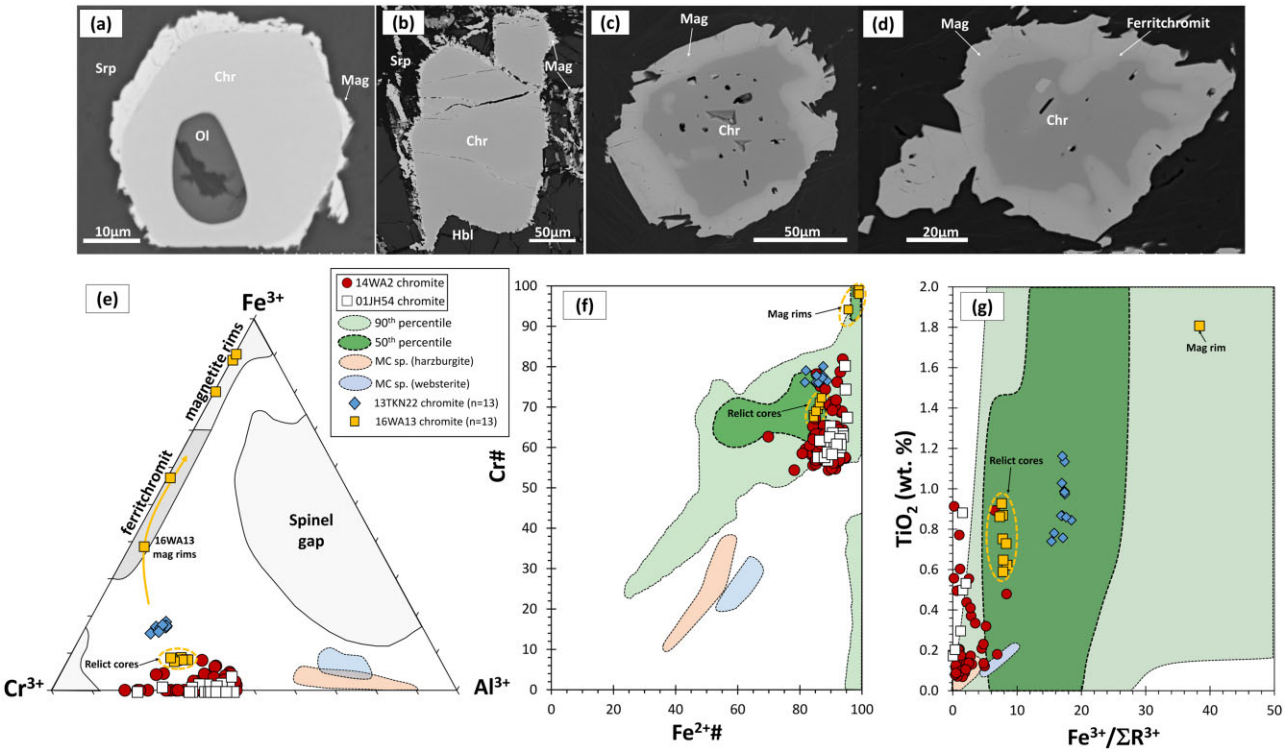

Fig. 14. Cr-spinel compositions from the Narryer Terrane. BSE images of Manfred Complex 13TKN22 chromite; (a) finer chromite (Chr) within 13TKN22, with a magnetite rim (Mag) and an inclusion of olivine (Ol); (b) coarser chromite within hornblende (Hbl). Serpentine (Srp) and magnetite (Mag) also shown. (c, d) Relict, porous chromite with thick ferritchromit and magnetite rims from 16WA13, an ultramafic rock from the SW limb of the Jack Hills belt. (Note the softening of the boundary between core and rim in comparison with 13TKN22.) (e–g) Compositional variability of 13TKN22 and 16WA13 chromite in comparison with Jack Hills detrital chromites. Spinel compositional fields from Manfred Complex (MC) harzburgites and websterites reported by Rowe & Kemp (2020) are included for comparison. Layered intrusion fields are from Barnes & Roeder (2001). (e) Cr^{3+}–Al^{3+}–Fe^{3+} triangular plot; (f) Cr# vs Fe^{2+}#; (g) TiO_2 vs $Fe^{3+}/\Sigma R^{3+}$.

Table 2: Representative EPMA compositions of 13TKN22 chromites and 16WA13 relict chromite cores

Sample:	13TKN22	13TKN22	13TKN22	16WA13	16WA13	16WA13
Grid ref. (UTM):	442851E 7076395N	442851E 7076395N	442851E 7076395N	489515E 7102336N	489515E 7102336N	489515E 7102336N
Crystal no.:	40	42	47			
Classification:	chromite	chromite	chromite	relict chromite	relict chromite	relict chromite
SiO_2	0.00	0.00	0.02	0.03	0.02	0.03
TiO_2	1.13	1.03	0.97	0.62	0.92	0.86
Al_2O_3	9.23	9.26	9.18	13.31	12.80	12.52
Cr_2O_3	43.66	44.18	43.87	45.96	46.48	46.77
V_2O_3	n.a.	n.a.	0.25	n.a.	n.a.	n.a.
Fe_2O_3	12.88	12.63	12.95	6.47	5.76	5.87
FeO	28.10	27.72	27.20	27.89	28.25	28.17
MgO	2.72	3.41	3.72	2.83	2.68	2.65
MnO	1.32	0.45	0.43	1.21	1.20	1.19
CaO	0.01	0.03	0.03	0.01	0.00	0.03
NiO	0.14	0.12	0.13	0.08	0.12	0.10
ZnO	0.60	0.59	0.58	1.08	1.06	1.08
Total	99.80	99.43	99.33	99.10	99.61	99.30
Mg#	14.73	17.99	14.59	13.00	12.49	12.37
Cr#	76.03	76.20	76.22	69.84	70.89	71.47
$Fe^{3+}/\Sigma Fe$	29.20	29.08	30.00	17.28	15.51	15.78
$Fe^{3+}/\Sigma R^{3+}$	17.59	17.18	17.64	8.56	7.72	7.86

V_2O_3 not analysed (n.a.) for some chromites within 13TKN22 and 16WA13. Fe_2O_3 calculated from AB_2O_4 stoichiometry using the equations of Droop (1987).

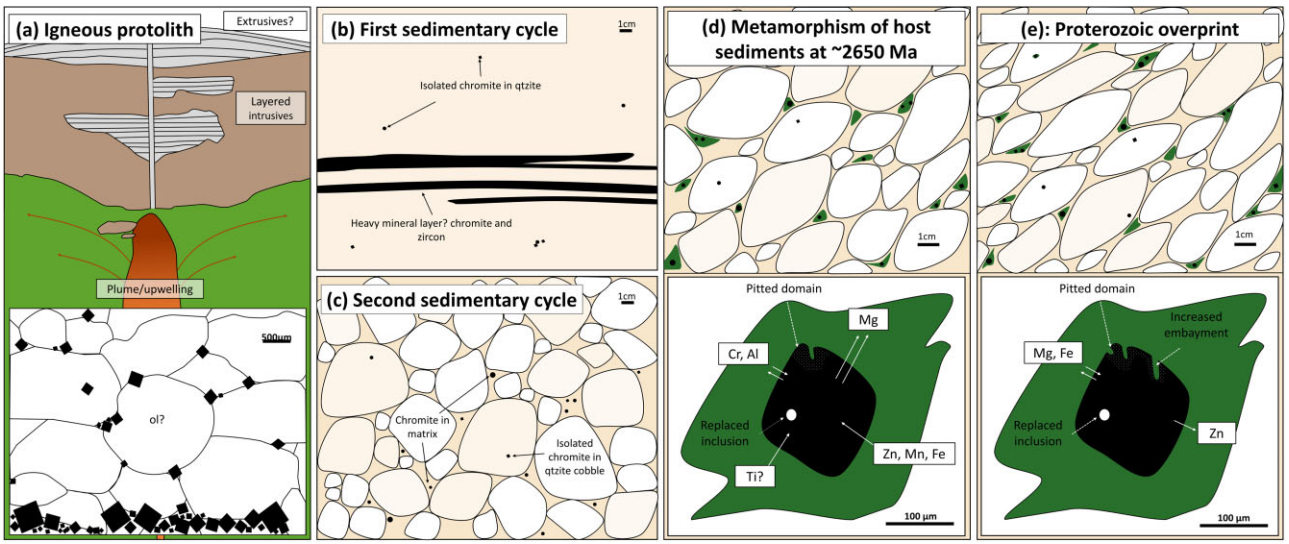

Fig. 15. Schematic representation of the geological history of Jack Hills chromites. (a) Original igneous crystallization in a spatially extensive igneous protolith, postulated to represent a single or multiple layered intrusion. (b) Exhumation and first sedimentary cycling event, with some chromites preserved isolated within quartzite. Chromites (± zircon) now observed within the matrix of Jack Hills metasedimentary rocks may have previously been preserved in heavy mineral layers or disseminated throughout quartzite. (c) Further sedimentary reworking in second cycling event deposits chromites in Jack Hills conglomerates and quartzites. Dispersion of chromites and zircons within both quartzite cobbles and matrix. (d) Metamorphism of Jack Hills metasedimentary rocks, probably representing peak upper greenschist to lower amphibolite facies metamorphism at ~2650 Ma. This event also formed fuchsite and other metamorphic assemblages within the host metasedimentary rock, replaced chromite primary inclusion assemblages, and led to exchange of chromite divalent cations with metamorphic fluids. (e) Proterozoic metamorphic overprint of metasedimentary rocks within the Jack Hills. Minor metamorphic exchange potentially indicated by zonation profiles.

deposition of Association 3 and 4 metasedimentary rocks (Fig. 2; Spaggiari, 2007; Spaggiari *et al.*, 2007). Although 16WA13 relict cores possess comparable Cr# to some Jack Hills detrital grains, gradational and lobate boundaries between relict cores and ferritchromit–magnetite rims, and their compositional trend towards magnetite (Fig. 14) are evidence for mobility of trivalent cations. This indicates that the Cr# values of 16WA13 chromite cores represent maximum values, and that comparisons should be made cautiously. However, further analyses of Jack Hills mafic and ultramafic rocks, particularly those preserved within lower strain areas, may prove more fruitful.

CONCLUSIONS

We have conducted a detailed textural and chemical investigation of detrital chromite from the Jack Hills, Western Australia, in a bid to expand beyond the intensively studied zircon record and provide additional perspectives on sources of sedimentary detritus (Fig. 15). Detrital chromites have undergone modification during metamorphism of host metasedimentary rocks, shown by increasingly homogenized and lowered Mg#, elevated ZnO and MnO, and partial to complete exchange of oxygen isotopes. Interaction with metamorphic fluids also resulted in the generation of pitted domains and replacement of primary mineral assemblages with metamorphic phases present in the matrix of host metasedimentary rocks, dominantly quartz and fuchsite. We propose that metamorphic modification coincided with peak upper greenschist to lower amphibolite facies metamorphism of Jack Hills metasedimentary rocks at ~2650 Ma.

Despite the development of fuchsite and high-Cr# domains, Jack Hills chromites yield a consistent range in Cr# across all samples and have limited intra-grain variability, indicating that the Cr# values of chromite cores are robust. An absence of ferritchromit rims on euhedral grains further argues against significant trivalent mobility prior to deposition. Critically, the moderate and variable Cr# of most detrital chromites suggests that komatiites or associated intrusive rocks were not a significant component of mafic–ultramafic crust within the erosional catchment of Jack Hills metasedimentary rocks. We propose a layered intrusive origin for Jack Hills detrital chromites, although we note that in the absence of further constraints from ferric iron and TiO_2 contents other sources cannot be excluded. It is currently unclear whether detrital chromites represent the remnants of a hitherto unknown intrusion(s), or were sourced from the 3730 Ma Manfred Complex or from ultramafic horizons within the Jack Hills belt. The lack of significant komatiite contribution may have geodynamic implications for eruption efficiencies within the catchment of Jack Hills sediments (e.g. heat-pipe versus 'plutonic squishy lid'; Moore & Webb, 2013; Rozel *et al.*, 2017) and, more broadly, the tectonic distribution of mafic and ultramafic crust within the Archean.

Although this study focused on Jack Hills detrital chromites, we have demonstrated that with a careful and detailed approach characteristics of the igneous

precursors of detrital chromites may be determined. However, we show that identification of key physicochemical signatures of chromite modification are critical to assess the veracity of interpretations derived from detrital chromites preserved within Archean metasedimentary rocks. Future studies of Archean detrital chromites should ideally be restricted to mature metasedimentary units that have undergone at most lower amphibolite facies metamorphism to minimize trivalent cation mobility. Where alteration of key physicochemical signatures can be shown to be absent, Cr# and Fe_2O_3 and TiO_2 contents may be used to provide significant insights into the provenance of mafic or ultramafic protoliths. Fuchsitic metasedimentary rocks are commonly reported within Archean terranes (e.g. Randive *et al.*, 2015), indicating that the eroded remnants of mafic and ultramafic crust are abundant. Detrital chromites within fuchsitic metasedimentary rocks may therefore represent an innovative tool in understanding the distribution of eroded Archean mafic and ultramafic crust, and yield important insights into geodynamic regimes of the early Earth.

ACKNOWLEDGEMENTS

L. G. Staddon wishes to thank Stuart Kearns and Ben Buse for their assistance with EPMA work, as well as Matthew Rowe and Chris Gray for their help during fieldwork in the Narryer Terrane. We are grateful to Tod Waight for editorial handling, and to Louise Schoneveld and two anonymous reviewers for thorough reviews that greatly improved the paper.

FUNDING

This work was supported by a Natural Environment Research Council (NERC) GW4+ Doctoral Training Partnership studentship (Grant number S117831-117) and British Geological Survey (BGS) University Funding Initiative (BUFI) sponsorship (Grant number S118481-101) to L.G.S. A.J.C. is partially supported by the Space Science and Technology Centre at Curtin University. J.W.V. is funded by the European Research Council (Synergy Grant number 856555) and the US National Science Foundation (EAR-1524336).

SUPPLEMENTARY DATA

Supplementary data are available at *Journal of Petrology* online

REFERENCES

Ahmed, A. H. & Surour, A. A. (2016). Fluid-related modifications of Cr-spinel and olivine from ophiolitic peridotites by contact metamorphism of granitic intrusions in the Ablah area, Saudi Arabia. *Journal of Asian Earth Sciences* **122**, 58–79.

Amelin, Y., Lee, D. C., Halliday, A. N. & Pidgeon, R. T. (1999). Nature of the Earth's earliest crust from hafnium isotopes in single detrital zircons. *Nature* **399**, 252–255.

Arai, S., Shimizu, Y., Ismail, S. A. & Ahmed, A. H. (2006). Low-*T* formation of high-Cr spinel with apparently primary chemical characteristics within podiform chromitite from Rayat. *Mineralogical Magazine* **70**, 499–508.

Arai, S., Okamura, H., Kadoshima, K., Tanaka, C., Suzuki, K. & Ishimaru, S. (2011). Chemical characteristics of chromian spinel in plutonic rocks: Implications for deep magma processes and discrimination of tectonic setting: Chromian spinel in plutonic rocks. *Island Arc* **20**, 125–137.

Arndt, N. T., Lesher, C. M. & Barnes, S. J. (2008). Brief descriptions of six classic komatiite occurrences. In: *Komatiite*. Cambridge: Cambridge University Press, pp. 16–52.

Ashwal, L. D. & Bybee, G. M. (2017). Crustal evolution and the temporality of anorthosites. Earth-Science Reviews **173**, 307–330.

Barkov, A. Y., Nixon, G. T., Levson, V. M., Martin, R. F. & Fleet, M. E. (2013). Chromian spinel from PGE-bearing placer deposits, British Columbia, Canada: Mineralogical associations and provenance. *Canadian Mineralogist* **51**, 501–536.

Barnes, S. J. (1998). Chromite in komatiites, I. Magmatic controls on crystallization and composition. *Journal of Petrology* **39**, 1689–1720.

Barnes, S. J. (2000). Chromite in komatiites, II. Modification during greenschist to mid-amphibolite facies metamorphism. *Journal of Petrology* **41**, 387–409.

Barnes, S. J. & Roeder, P. L. (2001). The range of spinel compositions in terrestrial mafic and ultramafic rocks. *Journal of Petrology* **42**, 2279–2302.

Bell, E. A. & Harrison, T. M. (2013). Post-Hadean transitions in Jack Hills zircons: a signal of the late heavy bombardment? *Earth and Planetary Science Letters* **364**, 1–11.

Bell, E. A., Harrison, T. M., Kohl, I. E. & Young, E. D. (2014). Eoarchean crustal evolution of the Jack Hills zircon source and loss of Hadean crust. *Geochimica et Cosmochimica Acta* **146**, 27–42.

Bell, E. A., Boehnke, P., Harrison, T. M. & Mao, W. L. (2015a). Potentially biogenic carbon preserved in a 4·1 billion-year-old zircon. *Proceedings of the National Academy of Sciences of the USA* **112**, 14518–14521.

Bell, E. A., Boehnke, P., Hopkins-Wielicki, M. D. & Harrison, T. M. (2015b). Distinguishing primary and secondary inclusion assemblages in Jack Hills zircons. *Lithos* **234–235**, 15–26.

Berger, J., Diot, H., Lo, K., Ohnenstetter, D., Femenias, O., Pivin, M., Demaiffe, D., Bernard, A. & Charlier, B. (2013). Petrogenesis of Archean PGM-bearing chromitites and associated ultramafic–mafic–anorthositic rocks from the Guelb el Azib layered complex (West African craton, Mauritania). *Precambrian Research* **224**, 612–628.

Borlina, C. S., Weiss, B. P., Lima, E. A., Tang, F., Taylor, R. J. M., Einsle, J. F., Harrison, R. J., Fu, R. R., Bell, E. A., Alexander, E. W., Kirkpatrick, H. M., Wielicki, M. M., Harrison, T. M., Ramezani, J. & Maloof, A. C. (2020). Reevaluating the evidence for a Hadean–Eoarchean dynamo. *Science Advances* **6**, eaav9634. doi:10.1126/sciadv.aav9634.

Burkhard, D. J. M. (1993). Accessory chromium spinels: Their coexistence and alteration in serpentinites. *Geochimica et Cosmochimica Acta* **57**, 1297–1306.

Byerly, B. L., Lowe, D. R., Drabon, N., Coble, M. A., Burns, D. H. & Byerly, G. (2018). Hadean zircon from a 3·3 Ga sandstone, Barberton greenstone belt, South Africa. *Geology* **46**, 967–970.

Cameron, E., Valley, J. W., Ortiz-Cordero, D., Kitajima, K. & Cavosie, A. J. (2016). Detrital Jack Hills zircon–quartz $\delta^{18}O$ analysis tests alteration of zircon and zircon inclusions. *Goldschmidt Conference Abstracts* **2016**, 349.

Cameron, E. N. (1979). Titanium-bearing oxide minerals of the critical zone of the eastern Bushveld Complex. *American Mineralogist* **64**, 140–150.

Campbell, I. H. & Murck, B. W. (1993). Petrology of the G and H Chromitite Zones in the Mountain View Area of the Stillwater Complex. *Journal of Petrology* **34**, 291–316.

Cassidy, K. F., Champion, D. C., Krapez, B., Barley, M. E., Brown, S. J. A., Blewett, R. S., Groenewald, N. B. & Tyler, I. M. (2006). A revised geological framework for the Yilgarn Craton. *Geological Survey of Western Australia, Record 2006/8, 1-8*.

Cavosie, A. J., Valley, J. W., Fournelle, J. & Wilde, S. A. (2002). Implications for sources of Jack Hills metasediments: detrital chromite. *Goldschmidt Conference Abstracts* **2002**, A125.

Cavosie, A. J., Wilde, S. A., Liu, D. Y., Weiblen, P. W. & Valley, J. W. (2004). Internal zoning and U–Th–Pb chemistry of Jack Hills detrital zircons: a mineral record of early Archean to Mesoproterozoic (4348–1576 Ma) magmatism. *Precambrian Research* **135**, 251–279.

Cavosie, A. J., Valley, J. W. & Wilde, S. A. (2005). Magmatic δ^{18}O in 4400–3900 Ma detrital zircons: A record of the alteration and recycling of crust in the Early Archean. *Earth and Planetary Science Letters* **235**, 663–681.

Cavosie, A. J., Valley, J. W. & Wilde, S. A. (2018). The oldest terrestrial mineral record: thirty years of research on Hadean Zircon from Jack Hills, Western Australia. In: van Kranendonk, M. J., Bennett, V. C. & Hoffmann, J. E. (eds) *Earth's Oldest Rocks*. Amsterdam: Elsevier, pp. 255–273.

Challis, A., Grapes, R. & Palmer, K. (1995). Chromian muscovite, uvarovite, and zincian chromite: Products of regional metasomatism in northwest Nelson, New Zealand. *Canadian Mineralogist* **33**, 1263–1284.

Chaudhuri, T., Wan, Y., Mazumder, R., Ma, M. & Liu, D. (2018). Evidence of Enriched, Hadean Mantle Reservoir from 4·2–4·0 Ga zircon xenocrysts from Paleoarchean TTGs of the Singhbhum Craton, Eastern India. *Scientific Reports* **8, 7079**.

Colás, V., González-Jiménez, J. M., Griffin, W. L., Fanlo, I., Gervilla, F., O'Reilly, S. Y., Pearson, N. J., Kerestedjian, T. & Proenza, J. A. (2014). Fingerprints of metamorphism in chromite: New insights from minor and trace elements. *Chemical Geology* **389**, 137–152.

Compston, W. & Pidgeon, R. T. (1986). Jack Hills, evidence of more very old detrital zircons in Western Australia. *Nature* **321**, 766–769.

Cox, M. A., Cavosie, A. J., Reddy, S. M., Bland, P. A., Valley, J. W. (2017). The hunt for shocked zircon in the Jack Hills: 21,000 and counting ... *Lunar and Planetary Science Conference 2017* 1402.

Crowley, J. L., Myers, J. S., Sylvester, P. J. & Cox, R. A. (2005). Detrital zircon from the Jack Hills and Mount Narryer, Western Australia: evidence for diverse >4·0 Ga source rocks. *Journal of Geology* **113**, 239–263.

Dare, M. S., Tarduno, J. A., Bono, R. K., Cottrell, R. D., Beard, J. S. & Kodama, K. P. (2016). Detrital magnetite and chromite in Jack Hills quartzite cobbles: further evidence for the preservation of primary magnetizations and new insights into sediment provenance. *Earth and Planetary Science Letters* **451**, 298–314.

Dharma Rao, C. V., Santosh, M., Sajeev, K. & Windley, B. F. (2013). Chromite–silicate chemistry of the Neoarchean Sittampundi Complex, southern India: implications for subduction-related arc magmatism. *Precambrian Research* **227**, 259–277.

Dhuime, B., Wuestefeld, A. & Hawkesworth, C. J. (2015). Emergence of modern continental crust about 3 billion years ago. *Nature Geoscience* **8**, 552–555.

Dick, H. J. B. & Bullen, T. (1984). Chromian spinel as a petrogenetic indicator in abyssal and alpine-type peridotites and spatially associated lavas. *Contributions to Mineralogy and Petrology* **86**, 54–76.

Dott, R. H. (2003). The importance of eolian abrasion in supermature quartz sandstones and the paradox of weathering vegetation-free landscapes. *Journal of Geology* **111**, 387–405.

Droop, G. (1987). A general equation for estimating Fe^{3+} concentrations in ferromagnesian silicates and oxides from microprobe analyses, using stoichiometric criteria. *Mineralogical Magazine* **51**, 431–435.

Dunn, S. J., Nemchin, A. A., Cawood, P. A. & Pidgeon, R. T. (2005). Provenance record of the Jack Hills metasedimentary belt: Source of the Earth's oldest zircons. *Precambrian Research* **138**, 235–254.

Evans, B. W. & Frost, B. R. (1975). Chrome-spinel in progressive metamorphism—a preliminary analysis. *Geochimica et Cosmochimica Acta* **39**, 959–972.

Fanlo, I., Gervilla, F., Colás, V. & Subias, I. (2015). Zn-, Mn- and Co-rich chromian spinels from the Bou-Azzer mining district (Morocco): constraints on their relationship with the mineralizing process. *Ore Geology Reviews* **71**, 82–98.

Fleet, M. E., Angeli, N. & Pan, Y. M. (1993). Oriented chlorite lamellae in chromite from the Pedra-Branca mafic–ultramafic complex, Ceara, Brazil. *American Mineralogist* **78**, 68–74.

Fletcher, I. R., Rosman, K. J. R. & Libby, W. G. (1988). Sm–Nd, Pb–Pb and Rb–Sr geochronology of the Manfred Complex, Mount Narryer, Western Australia. *Precambrian Research* **38**, 343–354.

Froude, D. O., Ireland, T. R., Kinny, P. D., Williams, I. S., Compston, W., Williams, I. R. & Myers, J. S. (1983). Ion microprobe identification of 4,100–4,200 Myr-old terrestrial zircons. *Nature* **304**, 616–618.

Gervilla, F., Padrón-Navarta, J. A., Kerestedjian, T., Sergeeva, I., González-Jiménez, J. M. & Fanlo, I. (2012). Formation of ferrian chromite in podiform chromitites from the Golyamo Kamenyane serpentinite, Eastern Rhodopes, SE Bulgaria: a two-stage process. *Contributions to Mineralogy and Petrology* **164**, 643–657.

Godel, B., Barnes, S. J., Gürer, D., Austin, P. & Fiorentini, M. L. (2013). Chromite in komatiites: 3D morphologies with implications for crystallization mechanisms. *Contributions to Mineralogy and Petrology* **165**, 173–189.

González-Jiménez, J. M., Kerestedjian, T., Proenza, J. A. & Gervilla, F. (2009). Metamorphism on Chromite Ores from the Dobromirtsi Ultramafic Massif, Rhodope Mountains (SE Bulgaria). *Geologica Acta* **7**, 413–429.

Grange, M. L., Wilde, S. A., Nemchin, A. A. & Pidgeon, R. T. (2010). Proterozoic events recorded in quartzite cobbles at Jack Hills, Western Australia: new constraints on sedimentation and source of >4 Ga zircons. *Earth and Planetary Science Letters* **292**, 158–169.

Groves, D. I., Barrett, F. M., Binns, R. A. & McQueen, K. G. (1977). Spinel phases associated with metamorphosed volcanic-type iron–nickel sulfide ores from Western Australia. *Economic Geology* **72**, 1224–1244.

Harrison, T. M. & Schmitt, A. K. (2007). High sensitivity mapping of Ti distributions in Hadean zircons. *Earth and Planetary Science Letters* **261**, 9–19.

Harrison, T. M., Trail, D., Schmitt, A. K. & Watson, E. B. (2007). Rutile ^{207}Pb–^{206}Pb ages in the Jack Hills quartzite, Western Australia. *Goldschmidt Conference Abstracts* **2008**, A383.

Harrison, T. M., Schmitt, A. K., McCulloch, M. T. & Lovera, O. M. (2008). Early (≥4·5 Ga) formation of terrestrial crust: Lu–Hf, δ^{18}O, and Ti thermometry results for Hadean zircons. *Earth and Planetary Science Letters* **268**, 476–486.

Harrison, T. M., Bell, E. A. & Boehnke, P. (2017). Hadean Zircon Petrochronology. *Reviews in Mineralogy and Geochemistry* **83**(**1**), 329.

Haugaard, R., Waterton, P., Ootes, L., Pearson, D. G., Luo, Y. & Konhauser, K. (2021). Detrital chromites reveal Slave craton's missing komatiite. *Geology* 49(9), 1079–1083.

Hodel, F., Macouin, M., Triantafyllou, A., Carlut, J., Berger, J., Rousse, S., Ennih, N. & Trindade, R. I. F. (2017). Unusual massive magnetite veins and highly altered Cr-spinels as relics of a Cl-rich acidic hydrothermal event in Neoproterozoic serpentinites (Bou Azzer ophiolite, Anti-Atlas, Morocco). *Precambrian Research* **300**, 151–167.

Hofmann, A. E., Valley, J. W., Watson, E. B., Cavosie, A. J. & Eiler, J. M. (2009). Sub-micron scale distributions of trace elements in zircon. *Contributions to Mineralogy and Petrology* **158**, 317–335.

Hopkins, M. D., Harrison, T. M. & Manning, C. E. (2008). Low heat flow inferred from >4 Gyr zircons suggests Hadean plate boundary interactions. *Nature* **456**, 493–496.

Hopkins, M. D., Harrison, T. M. & Manning, C. E. (2010). Constraints on Hadean geodynamics from mineral inclusions in >4 Ga zircons. *Earth and Planetary Science Letters* **298**, 367–376.

Hopkins, M. D., Harrison, T. M. & Manning, C. E. (2012). Metamorphic replacement of mineral inclusions in detrital zircon from Jack Hills, Australia: Implications for the Hadean Earth. *Geology* **40**, e281.

Iizuka, T., Horie, K., Komiya, T., Maruyama, S., Hirata, T., Hidaka, H. & Windley, B. F. (2006). 4·2 Ga zircon xenocryst in an Acasta Gneiss from northwestern Canada: evidence for early continental crust. *Geology* **34**, 245–248.

Iizuka, T., McCulloch, M. T., Komiya, T., Shibuya, T., Ohta, K., Ozawa, H., Sugimura, E. & Collerson, K. D. (2010). Monazite geochronology and geochemistry of meta-sediments in the Narryer Gneiss Complex, Western Australia: constraints on the tectonothermal history and provenance. *Contributions to Mineralogy and Petrology* **160**, 803–823.

Irvine, T. N. (1965). Chromian spinel as a petrogenetic indicator part 1: theory. *Canadian Journal of Earth Sciences* **2**, 648–672.

Irvine, T. N. (1967). Chromian spinel as a petrogenetic indicator part 2: petrologic application. *Canadian Journal of Earth Sciences* **4**, 71–103.

Kamber, B. (2015). The evolving nature of terrestrial crust from the Hadean, through the Archaean, into the Proterozoic. *Precambrian Research* **258**, 48–82.

Kamenetsky, V. S., Crawford, A. J. & Meffre, S. (2001). Factors controlling chemistry of magmatic spinel: an empirical study of associated olivine, Cr-spinel and melt inclusions from primitive rocks. *Journal of Petrology* **42**, 655–671.

Kamperman, M., Danyushevsky, L. V., Taylor, W. R. & Jablonski, W. (1996). Direct oxygen measurements of Cr-rich spinel: implications for spinel stoichiometry. *American Mineralogist* **81**, 1186–1194.

Kemp, A. I. S. (2018). Early earth geodynamics: cross examining the geological testimony. *Philosophical Transactions of the Royal Society of London, Series A* **376**, 20180169

Kemp, A. I. S., Wilde, S. A., Hawkesworth, C. J., Coath, C. D., Nemchin, A., Pidgeon, R. T., Vervoort, J. D. & DuFrane, S. A. (2010). Hadean crustal evolution revisited: New constraints from Pb–Hf isotope systematics of the Jack Hills zircons. *Earth and Planetary Science Letters* **296**, 45–56.

Kemp, A. I. S., Wilde, S. A. & Spaggiari, C. (2018). The Narryer Terrane, Yilgarn Craton, Western Australia: review and recent developments. In: van Kranendonk, M. J., Bennett, V. C. & Hoffmann, J. E. (eds) *Earth's Oldest Rocks*. Amsterdam: Elsevier, pp. 401–429.

Kimball, K. L. (1990). Effects of hydrothermal alteration on the compositions of chromian spinels. *Contributions to Mineralogy and Petrology* **105**, 337–346.

Kinny, P. D. & Nutman, A. P. (1996). Zirconology of the Meeberrie Gneiss, Yilgarn Craton, Western Australia: an early Archaean migmatite. *Precambrian Research* **78**, 165–178.

Kinny, P. D., Williams, I. S., Froude, D. O., Ireland, T. R. & Compston, W. (1988). Early Archean zircon ages from orthogneisses and anorthosites at Mount Narryer, Western Australia. *Precambrian Research* **38**, 325–341.

Kinny, P. D., Wijbrans, J. R., Froude, D. O., Williams, I. S. & Compston, W. (1990). Age constraints on the geological evolution of the Narryer Gneiss Complex, Western Australia. *Australian Journal of Earth Sciences* **37**, 51–69.

Langa, M. M., Jugo, P. J., Leybourne, M. I., Grobler, D. F., Adetunji, J. & Skogby, H. (2020). Chromite chemistry of a massive chromitite seam in the northern limb of the Bushveld Igneous Complex, South Africa: correlation with the UG-2 in the eastern and western limbs and evidence of variable assimilation of footwall rocks. *Mineralium Deposita* **56**, 31–44. doi:10.1007/s00126-020-00964-y.

Lenaz, D. & Princivalle, F. (2005). Crystal chemistry of detrital chromian spinel from the southeastern Alps and Outer Dinarides: The discrimination of supplies from areas of similar tectonic setting? *Canadian Mineralogist* **43**, 1305–1314.

Lowe, D. R., Drabon, N., Byerly, G. R. & Byerly, B. L. (2021). Windblown Hadean zircons derived by erosion of impact-generated 3·3 Ga uplifts, Barberton Greenstone Belt, South Africa. *Precambrian Research* **356**, 106111.

Lowry, D., Appel, P. W. U. & Rollinson, H. R. (2003). Oxygen isotopes of an early Archean layered ultramafic body, southern west Greenland: implications for magma source and post-intrusion history. *Precambrian Research* **126**, 273–288.

Marques, A. F. A., Barriga, F. J. A. S. & Scott, S. D. (2007). Sulfide mineralization in an ultramafic-rock hosted seafloor hydrothermal system: from serpentinization to the formation of Cu–Zn–(Co)-rich massive sulfides. *Marine Geology* **245**, 20–39.

Mondal, S. K., Ripley, E. M., Li, C., Ahmed, A. H., Arai, S., Liipo, J. & Stowe, C. (2003). Oxygen isotopic compositions of Cr-spinels from Archean to Proterozoic chromite deposits. *Goldschmidt Conference Abstracts* **2003**, A301.

Mondal, S. K., Ripley, E. M., Li, C. & Frei, R. (2006). The genesis of Archaean chromitites from the Nuasahi and Sukinda massifs in the Singhbhum Craton, India. *Precambrian Research* **148**, 45–66.

Moore, W. B. & Webb, A. A. G. (2013). Heat-pipe Earth. *Nature* **501**, 501–505.

Mukherjee, R., Mondal, S. K., Rosing, M. T. & Frei, R. (2010). Compositional variations in the Mesoarchean chromites of the Nuggihalli schist belt, Western Dharwar Craton (India): potential parental melts and implications for tectonic setting. *Contributions to Mineralogy and Petrology* **160**, 865–885.

Mukherjee, R., Mondal, S. K., González-Jiménez, J. M., Griffin, W. L., Pearson, N. J. & O'Reilly, S. Y. (2015). Trace-element fingerprints of chromite, magnetite and sulfides from the 3·1 Ga ultramafic–mafic rocks of the Nuggihalli greenstone belt, Western Dharwar craton (India). *Contributions to Mineralogy and Petrology* **169**, 59.

Myers, J. S. (1988a). Early Archean Narryer Gneiss Complex, Yilgarn Craton, Western Australia. *Precambrian Research* **38**, 297–307.

Myers, J. S. (1988b). Oldest known terrestrial anorthosite at Mount Narryer, Western Australia. *Precambrian Research* **38**, 309–323.

Myers, J. S. & Williams, I. R. (1985). Early Precambrian crustal evolution at Mount Narryer, Western Australia. *Precambrian Research* **27**, 153–163.

Nelson, D. R., Robinson, B. W. & Myers, J. S. (2000). Complex geological histories extending for ≥4·0 Ga deciphered from xenocryst zircon microstructures. *Earth and Planetary Science Letters* **181**, 89–102.

Nutman, A. P., Kinny, P. D., Compston, W. & Williams, I. S. (1991). SHRIMP U–Pb zircon geochronology of the Narryer Gneiss Complex, Western Australia. *Precambrian Research* **52**, 275–300.

Nutman, A. P., Bennett, V. C., Kinny, P. D. & Price, R. (1993). Large-scale crustal structure of the Northwestern Yilgarn Craton, Western Australia: Evidence from Nd isotopic data and zircon geochronology. *Tectonics* **12**, 971–981.

Pidgeon, R. T. & Nemchin, A. A. (2006). High abundance of early Archaean grains and the age distribution of detrital zircons in a sillimanite-bearing quartzite from Mt Narryer, Western Australia. *Precambrian Research* **150**, 201–220.

Pidgeon, R. T. & Wilde, S. A. (1998). The interpretation of complex zircon U–Pb systems in Archaean granitoids and gneisses from the Jack Hills, Narryer gneiss Terrane, Western Australia. *Precambrian Research* **91**, 309–332.

Power, M. R., Pirrie, D., Andersen, J. C. Ø. & Wheeler, P. D. (2000). Testing the validity of chrome spinel chemistry as a provenance and petrogenetic indicator. *Geology* **28**, 1027–1030.

Randive, K. R., Korakoppa, M. M., Muley, S. V., Varade, A. M., Khandare, H. W., Lanjewar, S. G., Tiwari, R. R. & Aradhi, K. K. (2015). Paragenesis of Cr-rich muscovite and chlorite in green-mica quartzites of Saigaon–Palasgaon area, Western Bastar Craton, India. *Journal of Earth System Science* **124**, 213–225.

Rasmussen, B., Fletcher, I. R., Muhling, J. R. & Wilde, S. A. (2010). *In situ* U–Th–Pb geochronology of monazite and xenotime from the Jack Hills belt: implications for the age of deposition and metamorphism of Hadean zircons. *Precambrian Research* **180**, 26–46.

Rasmussen, B., Fletcher, I. R., Muhling, J. R., Gregory, C. J. & Wilde, S. A. (2011). Metamorphic replacement of mineral inclusions in detrital zircon from Jack Hills, Australia: implications for the Hadean earth. *Geology* **39**, 1143–1146.

Roeder, P. L. (1994). Chromite: from the fiery rain of chondrules to the Kilauea lava lake. The Canadian Mineralogist **32**, 729–746.

Rollinson, H., Appel, P. W. U. & Frei, R. (2002). A metamorphosed, early Archaean chromitite from west Greenland: Implications for the genesis of Archaean anorthositic chromitites. *Journal of Petrology* **43**, 2143–2170.

Rollinson, H., Reid, C. & Windley, B. (2010). Chromitites from the Fiskenæsset Anorthositic Complex, West Greenland: clues to Late Archaean Mantle Processes. In: Kusky, T. M., Zhai, M.-G. & Xiao, W. (eds) *The Evolving Continents: Understanding Processes of Continental Growth. Geological Society, London, Special Publications* **338**, 197–212.

Rowe, M. L. & Kemp, A. I. S. (2020). Spinel, olivine, and pyroxene chemistry of the Eoarchaean Manfred Complex (Yilgarn Craton, Western Australia), with implications for the tectonic setting of Archaean layered mafic intrusions and the stabilisation of continental nuclei. *Lithos* 356–357, 105340.

Rozel, A., Golabek, G., Jain, C., Tackley, P. & Gerya, T. (2017). Continental crust formation on early Earth controlled by intrusive magmatism. *Nature* **545**, 332–338.

Sheppard, S. M. F. (1986). Characterization and Isotopic Variations in Natural Waters. *M.S.A. Reviews in Mineralogy* **16**, 165–184.

Schannor, M., Veksler, I. V., Hecht, L., Harris, C., Romer, R. L. & Manyeruke, T. D. (2018). Small-scale Sr and O isotope variations through the UG2 in the eastern Bushveld Complex: the role of crustal fluids. *Chemical Geology* **485**, 100–112.

Sharp, Z. D., Gibbons, J. A., Maltsev, O., Atudorei, V., Pack, A., Sengupta, S., Shock, E. L. & Knauth, L. P. (2016). A calibration of the triple oxygen isotope fractionation in the SiO2-H2O system and applications to natural samples. *Geochimica et Cosmochimica Acta* **186**, 105–119.

Shirey, S. B. & Walker, R. J. (1998). The Re–Os isotope system in cosmochemistry and high-temperature geochemistry. *Annual Review of Earth and Planetary Sciences* **26**, 423–500.

Spaggiari, C. V. (2007). Structural and lithological evolution of the Jack Hills greenstone belt, Narryer Terrane, Yilgarn Craton, Western Australia. *Western Australia Geological Survey, Record 2007/3* 49.

Spaggiari, C. V., Pidgeon, R. T. & Wilde, S. A. (2007). The Jack Hills greenstone belt, Western Australia—Part 2: Lithological relationships and implications for the deposition of >4·0 Ga detrital zircons. *Precambrian Research* **155**, 261–286.

Szilas, K., van Hinsberg, V., McDonald, I., Næraa, T., Rollinson, H., Adetunji, J. & Bird, D. (2018). Highly refractory Archaean peridotite cumulates: Petrology and geochemistry of the Seqi Ultramafic Complex. *Geoscience Frontiers* **9**, 689–714.

Tang, M., Chen, K. & Rudnick, R. (2016). Archean upper crust transition from mafic to felsic marks the onset of plate tectonics. *Science* **351**, 372–375.

Tarduno, J. A., Cottrell, R. D., Bono, R. K., Oda, H., Davis, W. J., Fayek, M., van't Erve, O., Nimmo, F., Huang, W., Thern, E. R., Fearn, S., Mitra, G., Smirnov, A. V. & Blackman, E. G. (2020). Paleomagnetism indicates that primary magnetite in zircon records a strong Hadean geodynamo. *Proceedings of the National Academy of Sciences of the USA* **117**, 2309–2318.

Turner, S., Wilde, S., Wörner, G., Schaefer, B. & Lai, Y.-J. (2020). An andesitic source for Jack Hills zircon supports onset of plate tectonics in the Hadean. *Nature Communications* **11**, 1241.

Valley, J. W., Kitchen, N., Kohn, M., Niendorf, C. R. & Spicuzza, M. J. (1995). UWG-2, a garnet standard for oxygen isotope ratios: strategies for high precision and accuracy with laser heating. *Geochimica et Cosmochimica Acta* **59**, 5223–5231.

Valley, J. W., Peck, W. H., King, E. M. & Wilde, S. A. (2002). A cool early Earth. *Geology* **30**, 351–354.

Valley, J. W., Cavosie, A. J., Shirey, S. B. & Wilde, S. A. (2005). 3·2 to 3·5 Ga Re–Os model ages for detrital chromite from Jack Hills, Western Australia: implications for Pilbara and Yilgarn Craton evolution. *American Geophysical Union, Fall Meeting 2005*, abstract #V21F-08.

Valley, J. W., Cavosie, A. J., Ushikubo, T., Reinhard, D. A., Lawrence, D. F., Larson, D. J., Clifton, P. H., Kelly, T. F., Wilde, S. A., Moser, D. E. & Spicuzza, M. J. (2014). Hadean age for a post-magma-ocean zircon confirmed by atom-probe tomography. *Nature Geoscience* **7**, 219–223.

Van Baalen, M. (1993). Titanium mobility in metamorphic systems—a review. *Chemical Geology* **110**, 233–249.

Wang, Q. & Wilde, S. A. (2018). New constraints on the Hadean to Proterozoic history of the Jack Hills belt, Western Australia. *Gondwana Research* **55**, 74–91.

Wilde, S. A., Valley, J. W., Peck, W. H. & Graham, C. M. (2001). Evidence from detrital zircons for the existence of continental crust and oceans on the Earth 4·4 Gyr ago. *Nature* **409**, 175–178.

Williams, I. R. & Myers, J. S. (1987). Archaean geology of the Mount Narryer region Western Australia. *Geological Survey of Western Australia: Report* **22**, 1–32.

Wood, B. J. & Virgo, D. (1989). Upper mantle oxidation-state: ferric iron contents of lherzolite spinels by ^{57}Fe Mössbauer-spectroscopy and resultant oxygen fugacities. *Geochimica et Cosmochimica Acta* **53**, 1277–1291.

Wyche, S. (2007). Evidence of Pre-3100 Ma crust in the Youanmi and South West Terranes, and Eastern Goldfields Superterrane, of the Yilgarn Craton. In: van Kranendonk, M. J., Smithies, R. H. & Bennett, V. C. (eds) *Earth's Oldest Rocks*. Amsterdam: Elsevier, pp. 113–124.

Wyche, S., Nelson, D. R. & Riganti, A. (2004). 4350–3130 Ma detrital zircons in the Southern Cross Granite–Greenstone Terrane, Western Australia: Implications for the early evolution of the Yilgarn Craton. *Australian Journal of Earth Sciences* **51**, 31–45.

Wylie, A. G., Candela, P. A. & Burke, T. M. (1987). Compositional zoning in unusual Zn-rich chromite from the Sykesville District of Maryland and its bearing on the origin of ferritchromit. *American Mineralogist* **72**, 413–422.

Zheng, Y.-F. (1991). Calculation of oxygen isotope fractionation in metal oxides. *Geochimica et Cosmochimica Acta* **55**, 2299–2307.